J. Fluid Mech. (2000), *vol.* 425, *pp.* 367–411. Printed in the United Kingdom

A similarity theory for the turbulent plane wall jet without external stream

By WILLIAM K. GEORGE[1], HANS ABRAHAMSSON[2], JAN ERIKSSON[3], ROLF I. KARLSSON[3], LENNART LÖFDAHL[1] AND MARTIN WOSNIK[4]†

[1]Chalmers University of Technology, S-412 96 Göteborg, Sweden

[2]Volvo Aero Corporation, SE-46181, Trollhätten, Sweden

[3]Vattenfall Utveckling AB, S-814 70 Älvkarleby, Sweden

[4]State University of New York at Buffalo, Buffalo, NY 14260, USA

(Received 12 July 1999 and in revised form 9 May 2000)

A new theory for the turbulent plane wall jet without external stream is proposed based on a similarity analysis of the governing equations. The asymptotic invariance principle (AIP) is used to require that properly scaled profiles reduce to similarity solutions of the inner and outer equations separately in the limit of infinite Reynolds number. Application to the inner equations shows that the appropriate velocity scale is the friction velocity, u_*, and the length scale is ν/u_*. For finite Reynolds numbers, the profiles retain a dependence on the length-scale ratio, $y^+_{1/2} = u_* y_{1/2}/\nu$, where $y_{1/2}$ is the distance from the wall at which the mean velocity has dropped to 1/2 its maximum value. In the limit as $y^+_{1/2} \to \infty$, the familiar law of the wall is obtained. Application of the AIP to the outer equations shows the appropriate velocity scale to be U_m, the velocity maximum, and the length scale $y_{1/2}$; but again the profiles retain a dependence on $y^+_{1/2}$ for finite values of it. The Reynolds shear stress in the outer layer scales with u_*^2, while the normal stresses scale with U_m^2. Also $U_m \sim y^n_{1/2}$ where $n < -1/2$ and must be determined from the data. The theory cannot rule out the possibility that the outer flow may retain a dependence on the source conditions, even asymptotically.

The fact that both these profiles describe the entire wall jet for finite values of $y^+_{1/2}$, but reduce to inner and outer profiles in the limit, is used to determine their functional forms in the 'overlap' region which both retain. The result from near asymptotics is that the velocity profiles in the overlap region must be power laws, but with parameters which depend on Reynolds number $y^+_{1/2}$ and are only asymptotically constant. The theoretical friction law is also a power law depending on the velocity parameters. As a consequence, the asymptotic plane wall jet cannot grow linearly, although the difference from linear growth is small.

It is hypothesized that the inner part of the wall jet and the inner part of the zero-pressure-gradient boundary layer are the same. It follows immediately that all of the wall jet and boundary layer parameters should be the same, except for two in the outer flow which can differ only by a constant scale factor. The theory is shown to be in excellent agreement with the experimental data which show that source conditions may determine uniquely the asymptotic state achieved. Surprisingly, only a single parameter, $B_1 = (U_m \nu/M_o)/(y_{1/2} M_o/\nu^2)^n = \text{constant}$ where $n \approx -0.528$, appears to be required to determine the entire flow for a given source.

---

† Present address: Chalmers University of Technology, 5–412 96 Göteborg, Sweden.

CONTENTS

1. Introduction

Turbulent wall jets have long been a favourite of experimenters and modellers, because of both their simple boundary conditions and their close resemblance to many flows of engineering importance. Such flows include applications in film cooling, ventilation, and separation control over wings, to cite but a few examples. An abundance of papers have been written about wall jets, and numerous review articles. The ones particularly of note with regard to this paper are by Launder & Rodi (1981, 1983) which provide excellent summaries of the state of knowledge to the early 1980s. Wygnanski, Katz & Horev (1992) (hereafter referred to as WKH) and Abrahamsson, Johansson & Löfdahl (1994) (hereafter referred to as AJL) both extend the reviews to the present, and provide more experimental data.

The flow under consideration is the plane wall jet with no externally imposed flow (figure 1). It is simulated in the laboratory by a jet of fluid from a high-aspect-ratio slot at the wall exhausting into a large chamber. In the ideal plane wall jet the flow is of infinite extent in the transverse (z) direction, and unconstrained in either the streamwise (x) or cross-stream (y) directions.

There has long been the suspicion that there should exist a similarity solution of some type for the plane wall jet; however, attempts to identify the solution have not been totally successful. Irwin (1973) tried to apply the single length and velocity scale methods presented in most text books, and had some success in scaling the outer mean velocity with the velocity maximum, U_m, and the velocity half-width, $y_{1/2}$. The scaling was less successful for the Reynolds stress, and no statement at all could be made about how the outer flow was coupled to the inner flow or what the friction law was, other than empirically. WKH were particularly critical of the use of the familiar law of the wall and log profiles from boundary layer theory for the near-wall region.

It might be asked: Who cares whether similarity solutions to the governing equations exist or not, since the wall jet flows of industrial interest do not satisfy these simple boundary conditions? The answer is the same as for any turbulent flow under

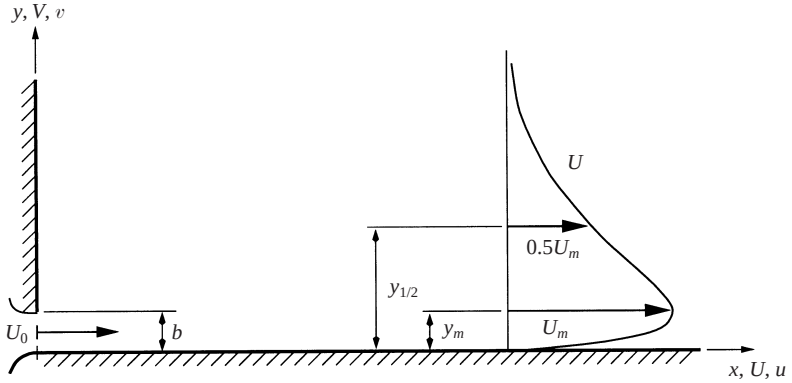

FIGURE 1. Schematic of the plane wall jet.

consideration. Only a similarity solution provides an unambiguous test of a turbulence model independent of computational constraints and experimental difficulties. It does not depend on computational grid, domain, or differencing schemes, nor does it depend on difficulties in realizing and measuring a laboratory flow. It exists independent of closure approximations, and thus the scaling laws it offers can be used to test closure hypotheses. Its straightforward boundary conditions are free from the finite limits of experimental facilities or computer memories, and thus its profiles provide an ideal reference for testing the effects of enclosure.

There have been four recent developments which make reconsideration of wall jet similarity theory timely. First, George (1989) showed that the single length and velocity scale approach to the similarity of free shear flows was almost never correct since it over-constrained the equations, and he proposed the more general approach which will be applied here. Second, George (1995), suggested an asymptotic invariance principle which not only could be applied to free shear flows, but allowed the inner and outer portions of boundary layer flows to be considered separately, then matched at *finite* Reynolds numbers. Third, George & Castillo (1997) successfully applied this approach to the zero-pressure-gradient boundary layer and correlated the results with boundary layer data. And fourth, Karlsson, Eriksson & Persson (1993*a*, *b*) (hereafter referred to as KEP) and Eriksson, Karlsson & Persson (1998) (hereafter referred to as EKP) have provided velocity measurements which resolve both the high-turbulence-intensity outer flow and the wall region down to $y^+ = 1$ using LDA. The latter provide, for the first time, direct determination of the wall shear stress without reference to the theories being tested.

This paper reconsiders the question of whether the plane wall jet should admit similarity solutions at all. The new theory proposed will be tested against wall jet experiments, and compared step-by-step with the corresponding theory for the zero-pressure-gradient boundary layer by George & Castillo (1997), hereafter referred to as GC. Experiments receiving particular attention will be those of KEP/EKP and AJL. The KEP/EKP experiments were carried out in a water tank at Vattenfall Utveckling AB using two-component burst-mode LDA with statistically uniform seeding. The AJL experiment used hot wires in an air facility at Chalmers.† Both experiments were carefully coordinated and achieved very similar inlet conditions.

† The KEP/EKP data are believed to be more accurate than the AJL data because of well-known hot-wire errors close to walls, and also in the high-intensity outer turbulent flow where local instantaneous flow reversal can occur. The hot-wire data, on the other hand, have less scatter than the LDA data, making it easier to sort out trends, especially in the second-moment data.

2. Governing equations and boundary conditions

The equation of motion and boundary conditions appropriate to a plane wall jet with constant properties at high Reynolds number are given by (Irwin 1973)

$$U\frac{\partial U}{\partial x}+V\frac{\partial U}{\partial y}=\frac{\partial}{\partial y}\left[\langle -uv\rangle+\nu\frac{\partial U}{\partial y}\right]-\left\{\frac{\partial}{\partial x}\left[\langle u^2\rangle-\langle v^2\rangle\right]\right\} \tag{2.1}$$

where $U\to 0$ as $y\to\infty$ and $U=0$ at $y=0$. This equation has been obtained by integrating the y-momentum equation across the boundary layer to eliminate the pressure. It is the same equation that governs both the plane free jet and the turbulent boundary layer at zero pressure gradient; only the boundary conditions are different.

Equation (2.1) can be integrated across the flow to yield the momentum integral equation given to second order by

$$\frac{\mathrm{d}}{\mathrm{d}x}\int_0^\infty [U^2+\langle u^2\rangle-\langle v^2\rangle]\mathrm{d}y=-\frac{\tau_w}{\rho}\equiv -u_*^2 \tag{2.2}$$

where τ_w is the wall shear stress and u_* is the friction velocity. If the flow indeed evolves free from other influences, equation (2.2) can be integrated from the source to yield

$$\int_0^\infty [U^2+\langle u^2\rangle-\langle v^2\rangle]\mathrm{d}y=M_o-\int_0^x\frac{\tau_w}{\rho}\mathrm{d}x' \tag{2.3}$$

where ρM_o is the rate at which momentum is added per unit length at the source. Thus unlike the plane free jet where the momentum integral is constant, for the plane wall jet there is a slow but continuous loss of momentum to the wall. And unlike the boundary layer, the supply of momentum driving the flow is finite.

The presence of the no-slip condition precludes the possibility of similarity solutions for the entire flow. The normal stresses in equation (2.1) are negligible to second order, and can be omitted for now with no loss of generality (in § 7 it will be shown from the Reynolds stress equations that they also scale in similarity variables). Therefore solutions are sought which asymptotically (at infinite Reynolds number) satisfy the following outer and inner equations and boundary conditions:

outer region

$$U\frac{\partial U}{\partial x}+V\frac{\partial U}{\partial y}=\frac{\partial}{\partial y}\left[\langle -uv\rangle\right] \tag{2.4}$$

where $U\to 0$ as $y\to\infty$;

inner (or near wall) region

$$0=\frac{\partial}{\partial y}\left[\langle -uv\rangle+\nu\frac{\partial U}{\partial y}\right] \tag{2.5}$$

where $U=0$ at $y=0$. The neglected terms in both inner and outer equations vanish identically only at infinite Reynolds number. However, there is nothing in the development of these equations which precludes their approximate validity from the time the flow undergoes transition.

Just as for the turbulent boundary layer, equation (2.5) for the inner region can be integrated to obtain

$$\langle -uv\rangle+\nu\frac{\partial U}{\partial y}=\frac{\tau_w}{\rho}\equiv u_*^2 \tag{2.6}$$

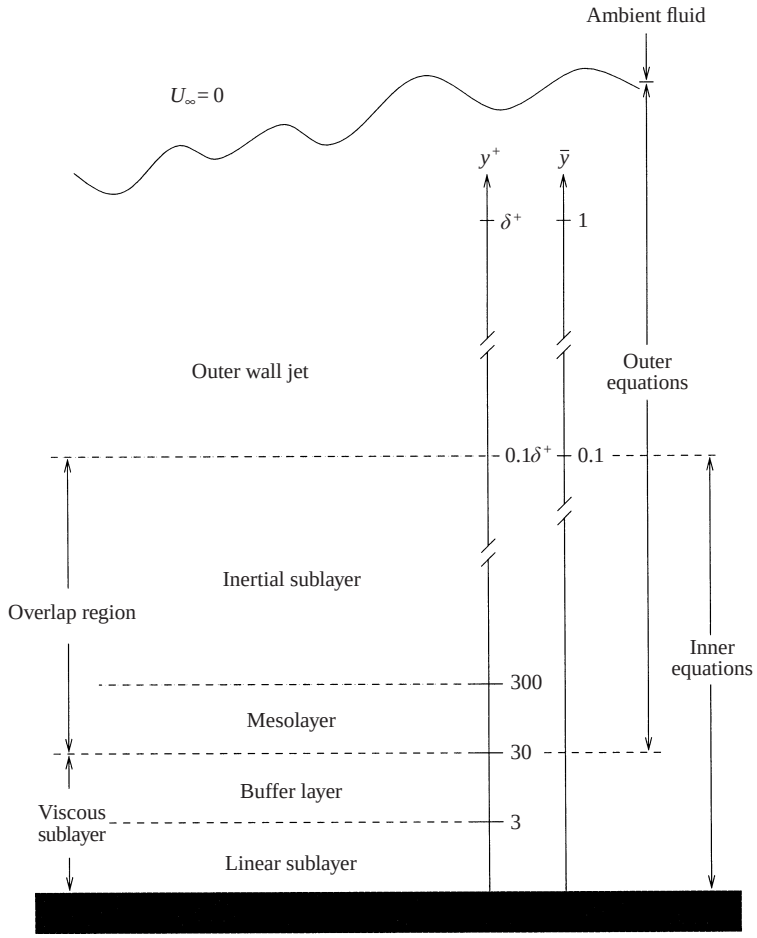

FIGURE 2. Schematic showing inner and outer regions together with subregions. (Here $\delta^+ \propto y^+_{1/2} = y_{1/2}u_*/\nu$.)

where τ_w is the wall shear stress and u_* is the corresponding friction velocity defined from it. It is clear that in the limit of infinite Reynolds number (but only in this limit) the total stress is constant across the inner layer, and hence its name 'constant stress layer'. The appearance of u_* in equation (2.6) does not imply that the wall shear stress is an independent parameter (like ν or M_o). It enters the problem only because it measures the forcing of the inner flow by the outer; or alternatively, it can be viewed as measuring the retarding effect of the inner flow on the outer. Thus u_* is a *dependent* parameter which must be determined by matching solutions of the inner and outer equations.

The inner and outer regions of the flow are illustrated schematically in figure 2, which also shows the subregions which will be identified later. As noted above, the inner layer occurs only because of the necessity of including viscosity in the problem so that the no-slip condition can be met. The outer layer, on the other hand, is dominated by inertia and the effects of viscosity enter primarily through the matching to the inner layer. Thus the outer flow is effectively governed by inviscid equations, but with *viscous-dominated inner boundary conditions* set by the inner layer.

3. The asymptotic invariance principle (AIP)

The traditional approach to the equations for the plane wall jet has been to ignore the presence of the wall and its effect on most of the flow, and to analyse the outer flow as a single length and velocity scale flow (Irwin 1973; Townsend 1976). George (1989) has pointed out that this method is too restrictive for even turbulent free shear flows since the Reynolds stresses should be allowed to have their own scales. GC extended this type of analysis to the zero-pressure-gradient turbulent boundary layer by considering the inner and outer equations separately. These equations ((2.4) and (2.5)), and therefore their similarity solutions, are exactly valid only in the limit of *infinite Reynolds number*. Seen another way, in the equations terms which are Reynolds number dependent are neglected, but these terms are truly gone only in the infinite Reynolds number limit. Therefore solutions to the full equations (as opposed to the inner and outer equations) must likewise be Reynolds number dependent and lose this dependence only at infinite Reynolds number. This idea was referred to as the *asymptotic invariance principle* by George (1995).

The asymptotic invariance principle (although not called by this name) has always been applied to free turbulent shear flows. Similarity solutions for those flows (when they exist) are infinite Reynolds number solutions because the equations from which they are derived are strictly valid only at infinite Reynolds number (George 1989; Tennekes & Lumley 1972). The difference in application here is that for the wall jet (like the boundary layer) there will be two sets of solutions – one which reduces to a full similarity solution of the outer equations at infinite Reynolds number, and another which reduces to a full similarity solution of the inner equations in the same limit. *For finite Reynolds numbers, the Reynolds number dependence of the equations themselves, however weak, dictates that the solutions cannot be similarity solutions anywhere.* But, as noted above, this is no different than for free shear flows which only asymptotically show Reynolds number independence.

In the following sections, the asymptotic invariance principle will be applied to some of the single-point equations governing the plane wall jet. Solutions will be sought which reduce to full similarity solutions of the equations in the limit of infinite Reynolds number, first for the inner equations and then for the outer. The form of these solutions will determine the appropriate scaling laws for finite as well as infinite Reynolds number, since alternative scaling laws could not be independent of Reynolds number in the limit. Once the method has been established by application to the equations governing the mean momentum, the same principle will be applied to equations governing the Reynolds stress equations and the statistical quantities appearing in them.

4. Full similarity of the inner equations

In keeping with the AIP set forth above, Similarity solutions to the infinite Reynolds number inner equations and boundary conditions are sought which are of the form

$$U = U_{si}(x) f_{i\infty}(y^+), \tag{4.1}$$

$$\langle -uv \rangle = R_{si}(x) r_{i\infty}(y^+), \tag{4.2}$$

where $y^+ \equiv y/\eta$ and the length scale $\eta = \eta(x)$ remains to be determined. The subscript $i\infty$ is used to distinguish these solutions to the limiting inner equation from the profiles for the entire flow (scaled with the same variables) that are introduced below.

Substitution into equation (2.6) and clearing terms yields

$$\left[\frac{u_*^2}{U_{si}^2}\right] = \left[\frac{R_{si}}{U_{si}^2}\right] r_{i\infty} + \left[\frac{\nu}{\eta U_{si}}\right] f'_{i\infty}. \tag{4.3}$$

All of the x-dependence is in the bracketed terms, therefore similarity is possible only if all of these have the same x-dependence, i.e.

$$\left[\frac{u_*^2}{U_{si}^2}\right] \sim \left[\frac{R_{si}}{U_{si}^2}\right] \sim \left[\frac{\nu}{\eta U_{si}}\right]. \tag{4.4}$$

Here the symbol $\sim$ is defined to mean 'has the same x-dependence as'.

Since three parameters are to be determined, and equation (4.4) gives only two independent conditions, one can be chosen arbitrarily. A convenient choice for η is

$$\eta = \nu/U_{si}. \tag{4.5}$$

Then the inner velocity scale must be the friction velocity so that

$$U_{si} \equiv u_*. \tag{4.6}$$

It follows that

$$\eta = \nu/u_*, \tag{4.7}$$

$$R_{si} = u_*^2. \tag{4.8}$$

Substitution into equation (4.3) yields the limiting inner momentum equation as

$$1 = r_{i\infty} + f'_{i\infty}. \tag{4.9}$$

The similarity variables derived above are the usual choices for the inner layer of a turbulent boundary layer, and have previously been used as scaling parameters for the wall jet by most investigators. For finite Reynolds number, however, the solutions for mean velocity and Reynolds stress will retain a Reynolds number dependence, no matter how they are scaled, since the Reynolds-averaged Navier–Stokes equations themselves do. It will be convenient later to represent this dependence symbolically by

$$u^+ \equiv \frac{U}{u_*} = f_i(y^+, \delta^+), \tag{4.10}$$

$$\frac{\langle -uv \rangle}{u_*^2} = r_i(y^+, \delta^+), \tag{4.11}$$

where $\delta^+ = \delta/\eta = u_*\delta/\nu$ is a Reynolds number to be defined later. Note that the evolution of the profiles with x which is not removed by the scaling parameters is accounted for by the dependence on δ^+ since $\delta = \delta(x)$ only. In the limit of infinite Reynolds number equations (4.10) and (4.11) reduce to similarity solutions of the inner equations. For finite Reynolds number they are simply a family of scaled profiles for the entire flow characterized by the parameter δ^+ (or $y^+_{1/2}$), like those shown in the plots below.

Figure 3 shows the mean velocity profile from the KEP data scaled in inner variables. These data collapse reasonably for y^+ less than 100 to 200 approximately, depending on distance downstream (or the Reynolds number). KEP and EKP have noted that the linear region next to the wall only extends to $y^+ \approx 3$. Outside this, the Reynolds shear stress begins to be important in the momentum balance until by $y^+ \approx 30$ it dominates the viscous stress completely. This region where the Reynolds

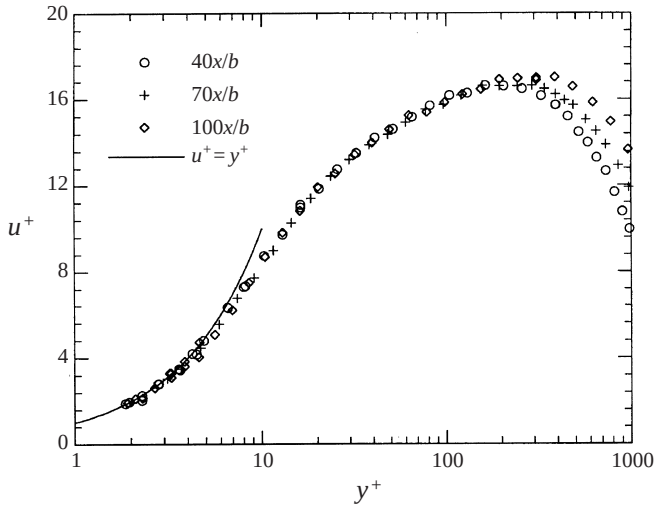

FIGURE 3. The mean velocity profile in inner scaling: KEP data at $40x/b$, $70x/b$ and $100x/b$.

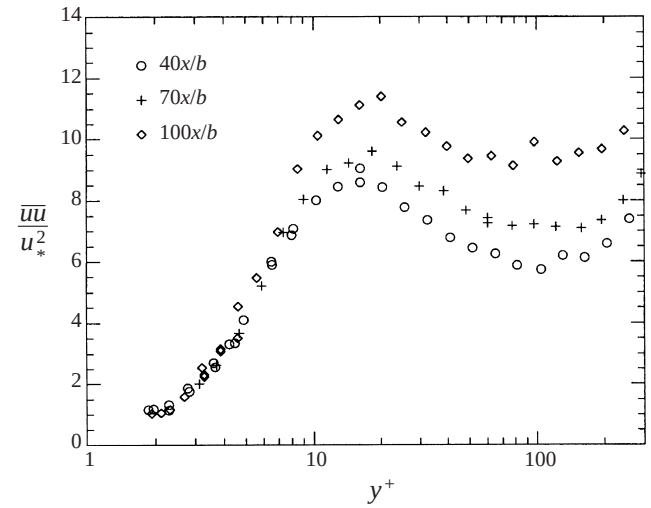

FIGURE 4. The streamwise normal Reynolds stress in inner scaling: KEP data at $40x/b$, $70x/b$ and $100x/b$.

shear stress and viscous stress are both important will be referred to as the *buffer region*. Figure 2 shows both the linear and buffer layers to comprise the viscous sublayer, so named since viscous stresses play a significant role in the single-point equations. Most importantly, convection effects by the mean velocity are negligible as long as $y_m^+ = y_m u_* / \nu \gg 30$.

Note that application of the AIP to the Reynolds stress equations near the wall shows that u_* and ν are the appropriate quantities for scaling all the single-point quantities. From figure 4 it is obvious that the inner scaling fails completely for $\langle u^2 \rangle$ outside $y^+ \approx 7$. Interestingly, this is the outer extent to which the fourth-order expansion of u^+ at the wall (i.e. $u^+ = y^+ + c_4 y^{+4}$) can adequately describe the mean velocity, cf. EKP and § 12. Both $\langle -uv \rangle$ and $\langle v^2 \rangle$ show similar tendencies as shown

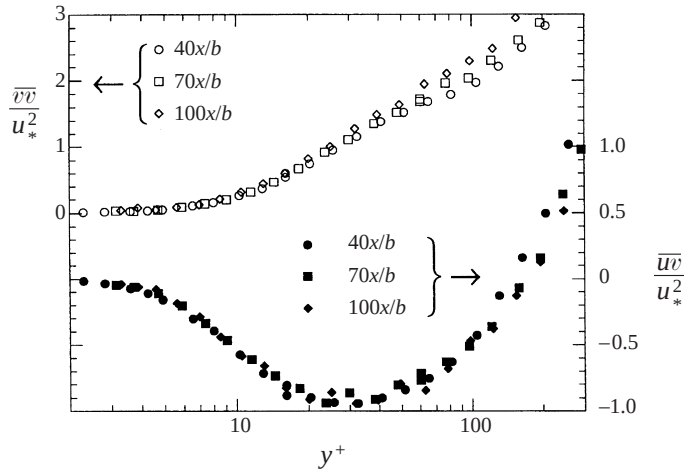

FIGURE 5. The cross-stream normal and shear Reynolds stress in inner scaling: KEP data at $40x/b$, $70x/b$ and $100x/b$.

in figure 5, but the curves do not separate as dramatically, perhaps because of the kinematic condition on v at the wall. These results are consistent with the conclusions of GC and Gad-el-Hak & Bandyopadhyay (1994) for the zero-pressure-gradient turbulent boundary layer.

5. Full similarity of the outer equations

In accordance with the asymptotic invariance principle, solutions to the outer momentum equation and boundary conditions are sought which reduce to similarity solutions of these equations in the limit of infinite Reynolds number:

$$U = U_{so} f_{o\infty}(\bar{y}), \tag{5.1}$$

$$-\langle uv \rangle = R_{so} r_{o\infty}(\bar{y}), \tag{5.2}$$

where $\bar{y} = y/\delta$ and U_{so}, R_{so}, and δ are functions of x only. It is important to note that, unlike in the previous analysis of Irwin (1973), *no scaling laws are assumed at the outset*, but will be derived from the conditions for similarity of the governing equations. In particular, it is not assumed that $R_{so} = U_{so}^2$. As before, the subscript $o\infty$ is used to distinguish these infinite Reynolds number solutions from the Reynolds-number-dependent profiles scaled in outer variables which will be used later. The velocity could have been written as a deficit using some reference velocity in the outer layer to avoid the necessity of accounting for its variation across the inner layer; however the results can be shown to be the same.

Substitution into equation (2.4) and clearing terms yields

$$\left[\frac{\delta}{U_{so}}\frac{\mathrm{d}U_{so}}{\mathrm{d}x}\right] f_{o\infty}^2 - \left(\left[\frac{\mathrm{d}\delta}{\mathrm{d}x}\right] + \left[\frac{\delta}{U_{so}}\frac{\mathrm{d}U_{so}}{\mathrm{d}x}\right]\right) f'_{o\infty} \int_0^{\bar{y}} f_{o\infty}(\xi)\mathrm{d}\xi = \left[\frac{R_{so}}{U_{so}^2}\right] r'_{o\infty}. \tag{5.3}$$

The V-component of velocity has been eliminated by integrating the continuity equation from the wall, thus introducing a contribution from the inner layer which vanishes identically at infinite Reynolds number. The only difference between this

equation and the one utilized by Irwin (1973) is the factor of $[R_{so}/U_{so}^2]$ on the right-hand side, but it will be seen to be very important below.

For the type of equilibrium similarity solution suggested by George (1989, 1995) to be possible, the bracketed terms must all have the same x-dependence. This is possible only if

$$\frac{1}{U_{so}}\frac{\mathrm{d}U_{so}}{\mathrm{d}x} \sim \frac{1}{\delta}\frac{\mathrm{d}\delta}{\mathrm{d}x} \tag{5.4}$$

and

$$R_{so} \sim U_{so}^2 \frac{\mathrm{d}\delta}{\mathrm{d}x}. \tag{5.5}$$

Note that Irwin (1973) assumed at the outset that $R_{so} = U_m^2$; this assumption is not justified. The Reynolds stress scale is not U_{so}^2, but an entirely different scale depending also on the growth rate, $\mathrm{d}\delta/\mathrm{d}x$. Thus the x-dependence of R_{so} is the same as U_{so}^2 only if the wall jet can be shown to grow linearly. It will be shown below that linear growth is not possible. It can also be shown (see Appendix B) that the inner and outer Reynolds shear stress can match (to first order) only if

$$R_{so} \sim U_{so}^2 \frac{\mathrm{d}\delta}{\mathrm{d}x} \sim u_*^2. \tag{5.6}$$

The need for such a matching is intuitively obvious, since the only non-zero boundary condition on the Reynolds stress in the outer flow is that imposed by the inner. Thus the outer flow is governed by two velocity scales. The similarity constraint of equation (5.4) is satisfied if U_{so} is a power of δ, i.e.

$$U_{so} \sim \delta^n, \tag{5.7}$$

where the coefficient and the exponent n remain to be determined, but can at most be a function of the source conditions. This is a specific prediction which is easy to test from experiment, but it does not seem to have been noticed previously. Note that equation (5.4) also implies that if the velocity scale varies as a power of distance, x, then δ must also vary as a power of x. But, contrary to popular assumption, there is no reason to believe *a priori* that either is true, nor will they be found to be except possibly asymptotically.

It is important to note that there is nothing in the equations to suggest that the bracketed terms of equation (5.3) must be the same for all flows. In other words, while all of the bracketed terms must have the same x-dependence and their ratios must be constant, in principle at least, the constants may vary from flow to flow. Thus, contrary to conventional wisdom, the equations themselves cannot rule out the possibility of an asymptotic dependence on the source (or initial) conditions.

An interesting feature of the mean velocity and Reynolds stress profiles can be seen by rewriting equation (5.3) using the similarity conditions as

$$nf_{o\infty}^2 - (1+n)f'_{o\infty}\int_0^{\bar{y}} f_{o\infty}(\xi)\mathrm{d}\xi = \left[\frac{R_{so}}{U_{so}^2 \mathrm{d}\delta/\mathrm{d}x}\right] r'_{o\infty} \tag{5.8}$$

The bracketed term on the right-hand side can be incorporated as a simple scale factor into the function $r_{o\infty}$ by defining

$$\tilde{r}_{o\infty} \equiv \left[\frac{R_{so}}{U_{so}^2 \mathrm{d}\delta/\mathrm{d}x}\right] r_{o\infty}. \tag{5.9}$$

Equation (5.8) then reduces further to

$$nf_{o\infty}^2 - (1+n)f'_{o\infty}\int_0^{\bar{y}} f_{o\infty}(\xi)\mathrm{d}\xi = \tilde{r}'_{o\infty} \tag{5.10}$$

The implications of this are striking:

(i) If the value of n is universal, then properly scaled mean velocity and Reynolds stress profiles from different wall jets must be exactly the same even if the x-dependence of $\mathrm{d}\delta/\mathrm{d}x$ is itself dependent on the initial conditions. Conversely, collapse of the profiles from different experiments means that n is universal, even if the other ratios depend on initial conditions.

(ii) In view of (i), the collapse of the properly scaled mean velocity and Reynolds shear stress profiles from different experiments cannot be taken to imply that the wall jet is asymptotically independent of its initial (or upstream) conditions. Such independence must be established from the other parameters, if it exists at all.

It should be noted that similar statements are not true, in general, for the other second-order and higher-moment profiles for which a simple scale change cannot make the profiles independent of source conditions. Thus the outer wall jet shares this characteristic with free shear flows (cf. George 1989). The data considered below will show that the exponent n appears to be universal; yet the asymptotic wall jet may still be dependent on its source conditions.

Since the only boundary conditions on U are homogeneous, the scale velocity U_{so} can be chosen as the maximum velocity, U_m with no loss of generality. Similarly, the outer length scale δ can be identified with any convenient location in the outer flow; hence it can hereafter be assumed with no loss of generality to be the familiar half-width denoted as $y_{1/2}$.† The extension of the AIP to the Reynolds stress equations in § 7 shows that some of the turbulence moments scale with U_m, some with u_*, and some with both. The normal stresses, $\langle u^2\rangle$, $\langle v^2\rangle$, and $\langle w^2\rangle$ scale as U_m^2; hence they are quite different from the Reynolds shear stress.

According to the AIP, the similarity scaling derived above is appropriate for finite Reynolds numbers as well, since only it can be invariant in the limit of infinite Reynolds number. Thus the velocity and Reynolds stress profiles in outer variables are

$$\frac{U}{U_m} = f_o(\bar{y}, y_{1/2}^+) \tag{5.11}$$

and

$$\frac{\langle -uv\rangle}{u_*^2} = r_o(\bar{y}, y_{1/2}^+), \tag{5.12}$$

where $\delta^+ \equiv y_{1/2}^+$ is the *local* Reynolds number. The profiles scaled in this manner, unlike their infinite Reynolds number limits, are valid for all y until the limit is taken. However, the scaled data can never collapse perfectly except in the limit, nor can they be made to collapse with any other Reynolds-number-independent scaling. Obviously f_o and r_o converge to $f_{o\infty}$ and $r_{o\infty}$, respectively, in the limit, and lose in the process their ability to describe the inner flow.

† Alternatively the outer length scale could have been identified with the position of the velocity maximum, say y_m, since it also occurs in the outer flow, at least if the Reynolds number is high enough. This choice has the disadvantage that it is difficult to determine the precise location of the maximum experimentally because of the slow variation of the velocity around it, quite unlike $y_{1/2}$ where the velocity is changing rapidly.

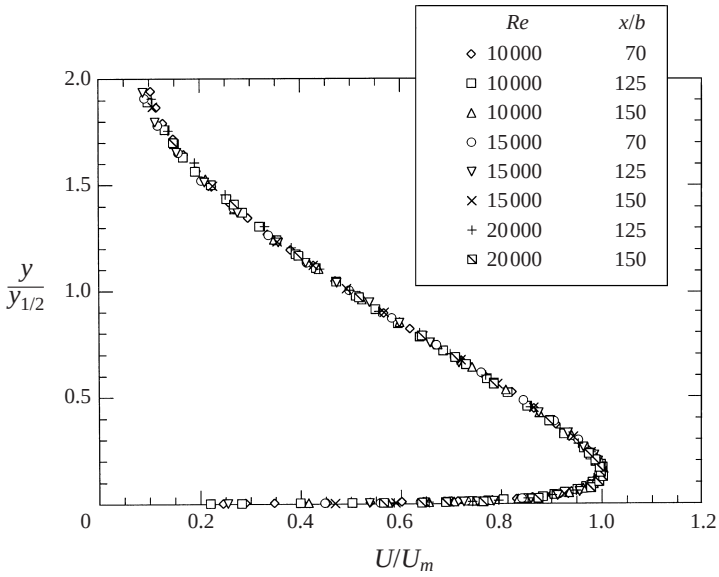

FIGURE 6. The mean velocity profile in outer scaling: AJL data at different inlet Reynolds numbers and streamwise positions.

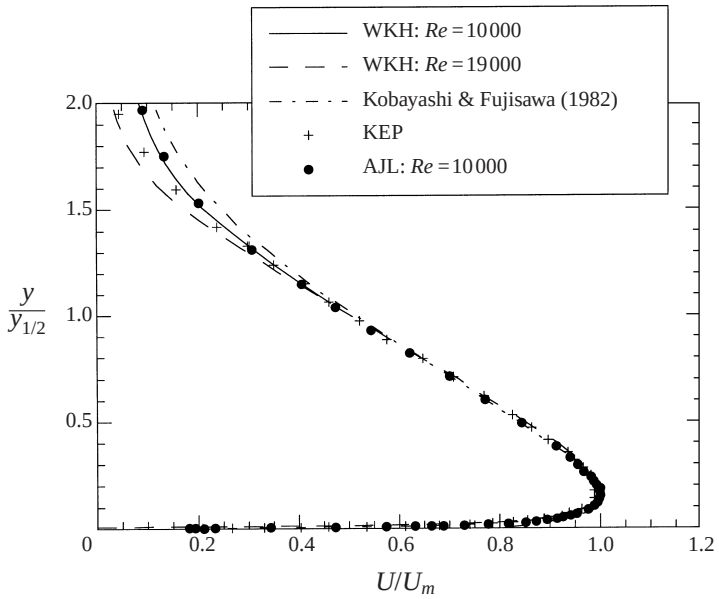

FIGURE 7. Comparison of mean velocity profiles of various investigators in outer variables.

6. Experimental verification of the outer flow analysis

Figure 6 shows the mean velocity data of AJL normalized by U_m and $y_{1/2}$ from $x/b = 70$ to 150 for three different source Reynolds numbers. Figure 7 shows mean velocity profiles from a number of investigators. Except for the extreme outer edge of the flow (beyond $y/y_{1/2} > 1.3$ or so) where external flows, counter-flows, and measurement errors dominate, all the normalized mean velocity profiles are virtually

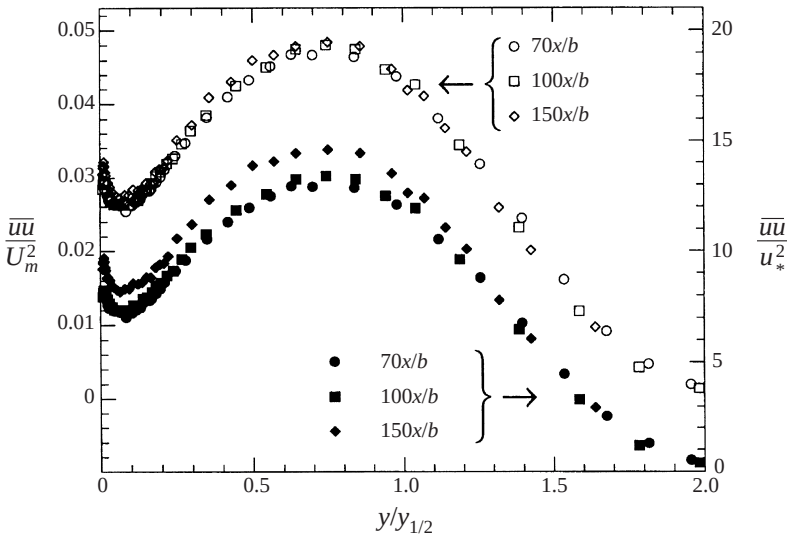

FIGURE 8. The streamwise normal Reynolds stress in outer scaling: AJL data at $70x/b$, $100x/b$ and $150x/b$.

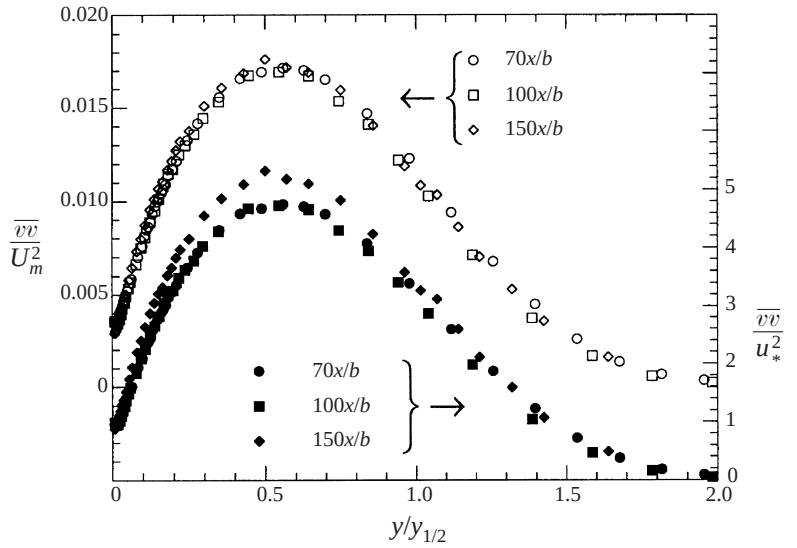

FIGURE 9. The cross-stream normal Reynolds stress in outer scaling: AJL data at $70x/b$, $100x/b$ and $150x/b$.

identical. This collapse has been observed by many before (e.g. AJL or see the review by Launder & Rodi 1981). The virtually identical profiles do imply that the exponent n in the similarity relation of equation (5.7) is universal. This will be corroborated below using $y_{1/2}$ and U_m. However, as noted above, they do not imply that the flow is independent of source conditions.

Figures 8, 9 and 10 show the Reynolds stresses of AJL normalized both by U_m^2, $y_{1/2}$ and by u_*^2, $y_{1/2}$. While the normal stresses collapse well in the outer flow with U_m^2, the Reynolds shear stress does not. On the other hand, the Reynolds shear stress collapses well with u_*^2, while the normal stresses do not. Thus both the mean velocity

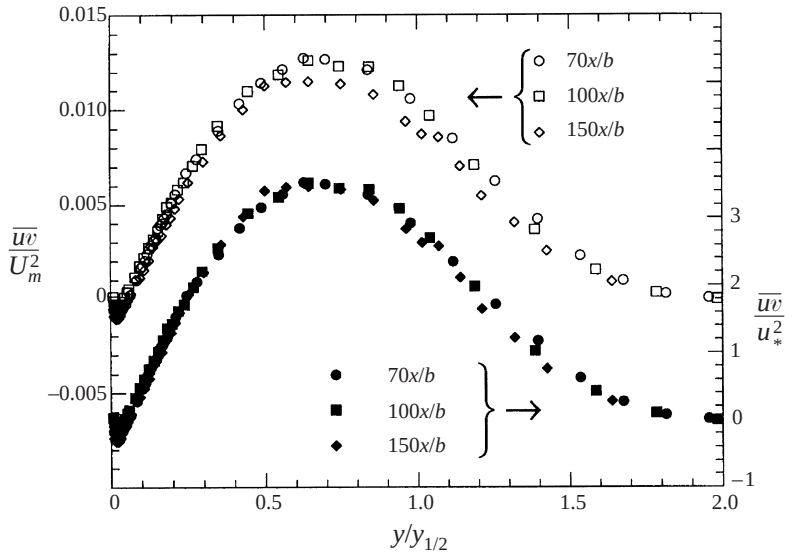

FIGURE 10. The Reynolds shear stress in outer scaling: AJL data at $70x/b$, $100x/b$ and $150x/b$.

and second moments are in striking agreement with the theory presented here. The differences are not as obvious for the LDA data of KEP for which there is not as much variation of u_*/U_m, perhaps due to the presence of the recirculation at the largest x/b values as noted by the authors. Both AJL and EKP show comparisons with several earlier experiments for all the second-order moments, and there are significant differences, both in profile shape and magnitude. While the latter may indeed represent a sensitivity to upstream conditions, the profile variations suggest that the differences may also be due to the well-known measurement problems with hot wires in such high-intensity flows and the manner in which the wires were employed. A definitive statement on this must await more extensive measurements with the more reliable LDA techniques (as in KEP).

Figure 11 shows a log-log plot of U_m/U_o versus $y_{1/2}/b$ for the data of KEP, AJL and WKH where U_o is the exit velocity at $x = 0$ and b is the width of the source. There is no theoretical justification for this normalization in spite of its widespread use; it does, however, collapse the data to within about 10%. All the data are in excellent agreement with the similarity requirement of a power law relation between U_m and $y_{1/2}$, i.e.

$$\frac{U_m}{U_o} = B_o \left[\frac{y_{1/2}}{b}\right]^n. \tag{6.1}$$

The line shown has slope $n = -0.528$ and $B_o = 1.09$, where the former was obtained from the momentum balance of the KEP data for $40 \leqslant x/b \leqslant 150$ (discussed in detail in § 14). The best fit slope, n, is nearly the same for all the curves, consistent with the apparently universal velocity profile noted above. The best fit values of B_o (assuming $n = -0.528$) are 1.10, 1.12, and 1.18 for the AJL data at source Reynolds numbers of 10 000, 15 000, and 20 000 respectively. Note that EKP have argued that their data should not all be treated equally because for small values of x/b the flow is still developing, while for $x/b > 100$ the flow is adversely influenced by the return flow in their facility. This will be discussed in §§ 14 and 15, and accounts for the slight deviation of the data from the momentum conservation value for large values of x/b.

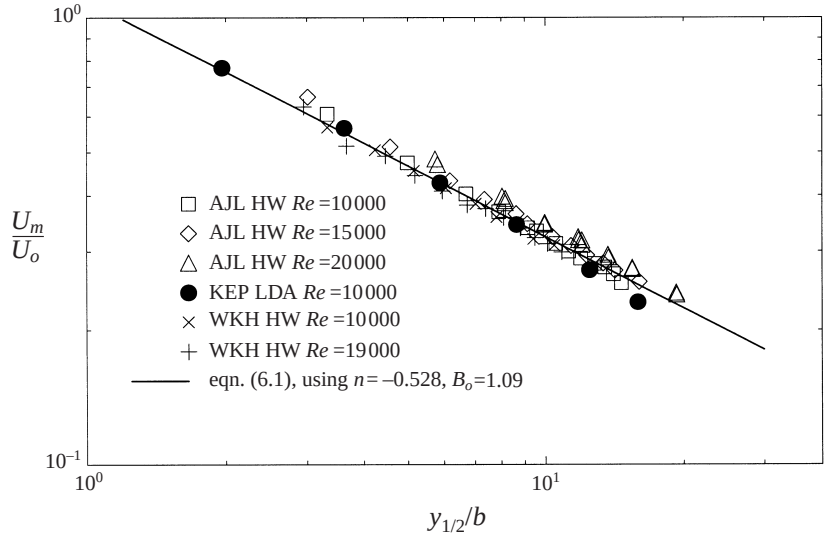

FIGURE 11. Log-log plot of U_m/U_o and $y_{1/2}/b$: KEP, AJL and WKH data.

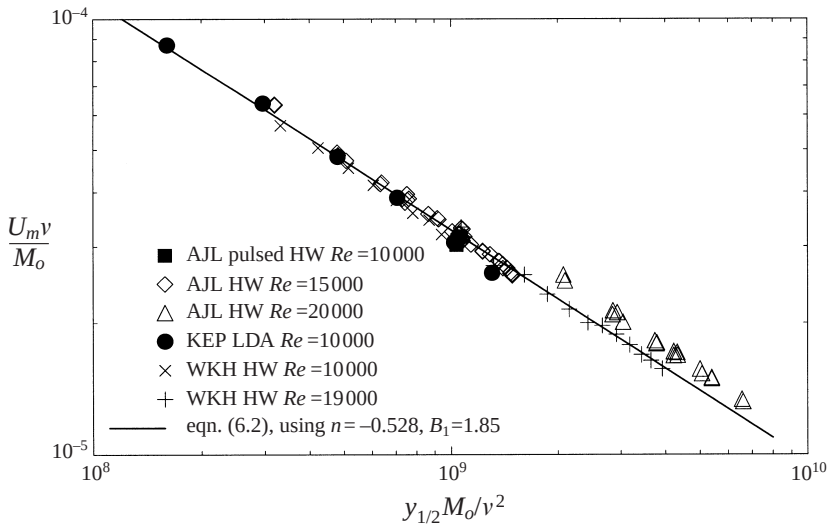

FIGURE 12. Log-log plot of vU_m/M_o versus $y_{1/2}M_o/v^2$: KEP, AJL and WKH data.

Some, but not all, of the dependence on source conditions can be eliminated by following Narasimha *et al.* (1973) (see also WKH) who suggested normalization by M_o and v where M_o is the rate at which momentum per unit mass per unit length is added at the source, since these would be the only parameters available for a line source of momentum. The same reasoning applied here (but without the additional assumption of a power law in x) yields a non-dimensionalized similarity condition as

$$\frac{vU_m}{M_o} = B_1 Y_{1/2}^n, \tag{6.2}$$

where $Y_{1/2}$ is defined as $Y_{1/2} \equiv y_{1/2}M_o/v^2$. Note that this normalization does not affect the exponent of the power law relationship between U_m and $y_{1/2}$, since it is already

dimensionless. Moreover, unlike power laws in x where the origin is arbitrarily chosen, there can be no virtual origin for $y_{1/2}$ since it evolves together with U_m.

It is important to recognize that while the scaling given by equation (6.2) is certainly the appropriate scaling for a line source of momentum, it should not be expected to collapse the data if finite source effects (like the exit profile or exit Reynolds number) are important. As noted earlier, there is nothing in the equations themselves to suggest that these finite source conditions are not important, and indeed the data appear to reflect that.

Figure 12 shows a log-log plot of the momentum–viscosity-normalized data from KEP, AJL and WKH. The line represents equation (6.2) using $B_1 = 1.85$ and $n = -0.528$, both determined from the momentum balance of the KEP data alone, again using only data for $40 \leqslant x/b \leqslant 150$. The best fit values for B_1 (assuming $n = -0.528$) are 1.87, 1.87 and 2.06 for the AJL 10 000, 15 000, and 20 000 data respectively. The corresponding values are 1.79 and 1.84 for the WKH data at source Reynolds numbers of 10 000 and 19 000 (the only WKH runs for which there was no imposed external stream). Note that the values inferred from the WKH data would be a percent or two higher if the momentum had been based on the actual exit profile instead of the top-hat inferred values. Also all of the hot-wire values of B_1 may already be about 8% too high because of the hot-wire errors in the determination of U_m and $y_{1/2}$ (about 2% and 12% respectively using the EKP results). Therefore it is impossible to tell whether these curves should indeed collapse, or whether each contains a unique dependence on its source. If the latter, the effect is not large, but (as will be seen later) still causes a noticeable variation in the rate at which the wall jet boundary layer grows.

As expected, the coefficient B_1 in the momentum/viscosity scaling shows a somewhat weaker source dependence than B_o using the source parameters b and U_o. Whether or not all of the sets of data are unique, it is obvious that they all individually satisfy the proper similarity power law relation between U_m and $y_{1/2}$. Moreover, even though the coefficient B_1 may show a slight dependence on the particular source and experiment, the value of n appears to be nearly (if not exactly) the same for all experiments.

In fact, B_1 should at least be exactly the same for a family of similar sources (i.e. same exit profile, Reynolds number, etc.) For a top-hat source B_1 and B_o are related by

$$B_o = B_1 \left(\frac{U_o b}{\nu} \right)^{(1+2n)} = B_1 R_o^{(1+2n)} \tag{6.3}$$

since $M_o = U_o^2 b$. All the experiments considered had approximately top-hat sources, which may explain why there is not a greater difference between figures 11 and 12.

All of the estimates for n from the individual data sets are within a few percent of each other. It will be argued later using the similarity form of the momentum integral, equation (14.5), that $n = -1/2$ must represent a limiting value, so for finite Reynolds numbers at least, $-n > 1/2$. Since n is close to $-1/2$ and enters the momentum balance as $(1 + 2n)$, the momentum balance is very sensitive to very small errors in n; hence the value of determining n from the momentum balance. The actual estimates for the individual downstream locations of the KEP data vary from $n = -0.526$ to $n = -0.536$, depending on how $\mathrm{d}y_{1/2}/\mathrm{d}x$ is estimated. The latter value is exactly the value obtained if the $M_o x/\nu^2$-dependence of the power law curve fits of WKH for $\nu U_m/M_o$ and $M_o y_{1/2}/\nu^2$ is eliminated to obtain equation (6.2), although the value of B_1 so obtained is lower by about 25%. Whether this variation represents a source

Reynolds number dependence, or is just an artifact of the method of analysis will require further investigation. Regardless of its precise value, the concurrent collapse of the normalized velocity profiles from all experiments suggests that the value of n may be universal, as noted above.

In summary, the collapse of the profiles as suggested by the theory (especially the Reynolds shear stress), the success of the similarity relation between $U_m \sim y_{1/2}^n$, and even the differences among different experiments provide strong experimental support for the proposed outer scaling. The latter point is especially important in view of the increasing number of flows which appear to retain asymptotically a dependence on initial conditions. Although GC suggested the possibility of such a dependence for the outer part of the zero-pressure-gradient boundary layer, the data were insufficient to make a judgement (although there were clues). There are, however, numerous examples of homogeneous and free shear flows which do appear to behave in this manner, e.g. isotropic decay (George 1992), homogeneous shear flow (George & Gibson 1992), plane wake (Wygnanski, Champagne & Marasli 1986), time-dependent wake (Moser, Rogers & Ewing 1998). But the wall jet appears to be the first wall-bounded flow for which it can be substantiated that initial conditions may matter, at least to the outer flow. And if the initial conditions matter, as will be seen in § 14, they can have an effect on the asymptotic spreading rate.

7. Scaling of the other turbulence quantities

For the inner layer, there is only one velocity scale, u_*, which enters the single-point equations; therefore all single-point statistical quantities must scale with it. This is, of course, the conventional wisdom, but with an important difference: the inner layer ends about $y^+ \approx 7$, not far from where the velocity profile ceases to be linear ($y^+ \approx 3$)! This is contrary to the usual practice to include the overlap layer as part of the wall layer. As shown before, the dependent variables in the overlap layer are expected to be functions of both inner and outer scales, and thus Reynolds number dependent. (Note that different considerations must be applied to the multi-point equations since conditions at a point can depend on those at another, and in particular those at a distance.)

From the preceding analysis, it is apparent that the outer wall jet at finite Reynolds numbers is governed by not one, but two velocity scales. In particular, the mean velocity and its gradients scale with U_m, while the Reynolds shear stress scales with u_*^2. Therefore it is not immediately obvious how the remaining turbulence quantities should scale. In particular, do they scale with U_m or u_*, or both? If the latter, then quantities scaled in the traditional way with only one of them will exhibit a Reynolds number dependence and will not collapse, even in the limit of infinite Reynolds number. It has already been noted in the plots of the previous section that this is indeed the case.

In view of the plots of the preceding section, it is reasonable to inquire under what conditions the equations for other turbulence quantities admit fully similar solutions. For the outer part of the wall jet at high Reynolds number, the equation for $\langle u^2 \rangle$ can be written (Tennekes & Lumley 1972) as

$$U\frac{\partial\langle u^2\rangle}{\partial x} + V\frac{\partial\langle u^2\rangle}{\partial y} = 2\left\langle \frac{p}{\rho}\frac{\partial u}{\partial x}\right\rangle + \frac{\partial}{\partial y}\left\{-\langle u^2 v\rangle\right\} - 2\langle uv\rangle\frac{\partial U}{\partial y} - 2\epsilon_u, \qquad (7.1)$$

where ϵ_u is the energy dissipation rate for $\langle u^2 \rangle$ and the viscous transport term has been neglected.

An order of magnitude analysis reveals the mean convection and turbulence transport terms to be of second order in the turbulence intensity u'/U, so to first order the equation reduces to simply a balance between production, dissipation and pressure strain rate. It could then be argued that these second-order terms should be neglected in the subsequent analysis, cf. Townsend (1976). It is precisely these second-order terms, however, that distinguish one boundary layer type flow from another, or from homogeneous flows (like channels and pipes) for that matter. Therefore, for a theory which purports to represent growing shear layers like the wall jet, they must be retained.

Similarity representations are sought for the new moments of the form

$$\tfrac{1}{2}\langle u^2 \rangle = K_u(x) k_u(\bar{y}), \tag{7.2}$$

$$\left\langle \frac{p}{\rho} \frac{\partial u}{\partial x} \right\rangle = P_u(x) p_u(\bar{y}), \tag{7.3}$$

$$-\tfrac{1}{2}\langle u^2 v \rangle = T_{u^2 v}(x) t_u(\bar{y}), \tag{7.4}$$

$$\epsilon_u = D_u(x) d_u(\bar{y}). \tag{7.5}$$

Similarity of the $\langle u^2 \rangle$-equation is possible only if†

$$K_u \sim U_m^2, \tag{7.6}$$

$$P_u \sim \frac{U_m^3}{\delta} \frac{\mathrm{d}\delta}{\mathrm{d}x}, \tag{7.7}$$

$$T_{u^2 v} \sim U_m^3 \frac{\mathrm{d}\delta}{\mathrm{d}x}, \tag{7.8}$$

$$D_u \sim \frac{U_m^3}{\delta} \frac{\mathrm{d}\delta}{\mathrm{d}x}. \tag{7.9}$$

All of these are somewhat surprising: the first (even though a second moment like the Reynolds stress) because the factor of $\mathrm{d}\delta/\mathrm{d}x$ is absent; the second, third and fourth because it is present.

Similar equations can be written for $\langle v^2 \rangle$ and $\langle w^2 \rangle$ i.e.

$$U \frac{\partial \langle v^2 \rangle}{\partial x} + V \frac{\partial \langle v^2 \rangle}{\partial y} = 2 \left\langle \frac{p}{\rho} \frac{\partial v}{\partial y} \right\rangle + \frac{\partial}{\partial y} \left\{ -\langle v^3 \rangle - 2\langle pv \rangle \right\} - 2\epsilon_v, \tag{7.10}$$

$$U \frac{\partial \langle w^2 \rangle}{\partial x} + V \frac{\partial \langle w^2 \rangle}{\partial y} = 2 \left\langle \frac{p}{\rho} \frac{\partial w}{\partial z} \right\rangle + \frac{\partial}{\partial y} \left\{ -\langle w^2 v \rangle \right\} - 2\epsilon_w. \tag{7.11}$$

When each of the terms in these equations is expressed in similarity variables, the resulting similarity conditions are

$$D_v \sim P_v \sim \frac{U_m K_v}{\delta} \frac{\mathrm{d}\delta}{\mathrm{d}x}, \tag{7.12}$$

$$D_w \sim P_w \sim \frac{U_m K_w}{\delta} \frac{\mathrm{d}\delta}{\mathrm{d}x}, \tag{7.13}$$

† Recall that the symbol $\sim$ is used herein to mean 'has the same x-dependence as', and should not be confused with 'order of magnitude'.

$$T_{v^3} \sim \frac{U_m K_v}{\delta}\frac{\mathrm{d}\delta}{\mathrm{d}x}, \tag{7.14}$$

$$T_{w^2 v} \sim \frac{U_m K_w}{\delta}\frac{\mathrm{d}\delta}{\mathrm{d}x}. \tag{7.15}$$

There is an additional equation which must be accounted for; namely that the sum of the pressure strain-rate terms in the component energy equations be zero (from continuity). Thus, in similarity variables,

$$P_u(x)p_u(\bar{y}) + P_v(x)p_v(\bar{y}) + P_w(x)p_w(\bar{y}) = 0. \tag{7.16}$$

This can be true for all $\bar{y}$ only if

$$P_u \sim P_v \sim P_w. \tag{7.17}$$

An immediate consequence is that

$$D_u \sim D_v \sim D_w \sim D_s \sim \frac{U_m u_*^2}{\delta}, \tag{7.18}$$

where D_s is the scale for the entire dissipation.

From equations (7.7), (7.12) and (7.13) it follows that the constraint imposed by (7.17) can be satisfied only if

$$K_u \sim K_v \sim K_w \sim U_m^2. \tag{7.19}$$

Thus all of the Reynolds normal stresses scale with U_m^2, and not with u_*^2 like the Reynolds shear stresses. But this is exactly what was observed in figures 8 and 9.

The remaining equation for the Reynolds shear stress is given by

$$U\frac{\partial\langle uv\rangle}{\partial x} + V\frac{\partial\langle uv\rangle}{\partial y} = \left\langle \frac{p}{\rho}\left(\frac{\partial u}{\partial y} + \frac{\partial v}{\partial x}\right)\right\rangle + \frac{\partial}{\partial y}\left\{-\langle uv^2\rangle\right\} - \langle v^2\rangle\frac{\partial U}{\partial y}. \tag{7.20}$$

This does not introduce any new similarity functions, but as in the boundary layer analysis of GC, it does create an interesting problem. The x-dependence of the last term (which is the leading-order term) is proportional to $(U_m R_{so}/\delta)\mathrm{d}\delta/\mathrm{d}x \sim (U_m^3/\delta)(\mathrm{d}\delta/\mathrm{d}x)^2$. If both terms are required to have the same x-dependence, a new constraint is imposed on the ones which already exist, namely

$$K_v \sim R_{so}\frac{\mathrm{d}\delta}{\mathrm{d}x} \sim U_m^2\left(\frac{\mathrm{d}\delta}{\mathrm{d}x}\right)^2 \sim u_*^2\frac{\mathrm{d}\delta}{\mathrm{d}x}. \tag{7.21}$$

Recall that R_{so} is only asymptotically equal to u_*^2 (from the matching), so the entire Reynolds shear stress scale evolves to this limit with increasing Reynolds number. Regardless, there is an apparent contradiction between equation (7.21) and equation (7.19). There are two possibilities for its resolution:

Either, the two conditions together require that in the limit of infinite Reynolds number,

$$\frac{\mathrm{d}\delta}{\mathrm{d}x} \sim \frac{u_*^2}{U_m^2} \sim \text{constant}. \tag{7.22}$$

Or, the term which creates the contradiction must go to zero faster than the other terms so the offending condition does not remain in the analysis. In fact, as for the boundary layer, the possibility for this occurs since the terms on the left-hand side of equation (7.20) are of order $(\mathrm{d}\delta/\mathrm{d}x)^2 \sim (u_*/U_m)^4$ relative to the leading term, whereas the highest-order terms in the normal stress equations are of order

$(\mathrm{d}\delta/\mathrm{d}x) \sim (u_*/U_m)^2$. Therefore the mean convection terms in the Reynolds shear stress equation will vanish faster in the limit of infinite Reynolds number than the remaining terms in any of the Reynolds stress equations if $\mathrm{d}\delta/\mathrm{d}x \to 0$.

It will be seen later that $\mathrm{d}\delta/\mathrm{d}x \to 0$ is a necessary condition for ensuring that the proper infinite Reynolds number dissipation limits can be satisfied, namely that the local dissipation rate be finite. Therefore equation (7.22) is not relevant, nor must it be satisfied.

It is clear from the above that the outer Reynolds stress equations indeed admit similarity solutions in the infinite Reynolds number limit (to second order in u_*/U_m), just as the mean momentum equations (and just as for the boundary layer). It is also clear from the figures shown earlier that the Reynolds stresses show a trend toward collapse in a manner consistent with the analysis above, even for the modest Reynolds numbers of the experiments. As noted earlier, nothing in the analysis or the data suggests that this similarity state should be independent of upstream and source conditions.

8. The overlap layer

Since both inner and outer similarity forms are non-dimensional profiles with different scales and the ratio of the scales is Reynolds number dependent, any region between the two similarity regimes cannot be Reynolds number independent, except asymptotically. As noted earlier, however, both inner and outer scaled profiles, f_i and f_o, describe the entire flow as long as the argument $\delta^+ = \delta/\eta$ is finite. Therefore at finite Reynolds numbers, both equations (4.10) and (5.11) must describe the region between the two similarity regimes. Thus the situation here is quite different from the usual asymptotic matching problem where infinite Reynolds number inner and outer solutions are extended and matched in an overlap region. Here both solutions are valid everywhere, at least for finite Reynolds numbers. Hence the objective is not to see if they overlap and match them if they do; rather, it is to determine whether the fact that they degenerate at infinite Reynolds number in different ways determines their functional forms in the common region they describe.

There are several pieces of information about the two profiles which can be utilized in this determination without further assumptions.

First, since both inner and outer forms of the velocity profile must describe the flow everywhere as long as the ratio of length scales, $\delta^+ = \delta/\eta$, is finite, it follows from equations (4.10) and (5.11) that

$$f_o(\bar{y}, \delta^+) = g(\delta^+) f_i(y^+, \delta^+), \tag{8.1}$$

where $g(\delta^+)$ has been defined as

$$g(\delta^+) \equiv u_*/U_m. \tag{8.2}$$

Second, for finite values of δ^+, the velocity derivatives from both forms of the velocity must also be the same everywhere. This requires

$$\frac{\bar{y}}{f_o}\frac{\mathrm{d}f_o}{\mathrm{d}\bar{y}} = \frac{y^+}{f_i}\frac{\mathrm{d}f_i}{\mathrm{d}y^+} \tag{8.3}$$

for all values of δ^+ and y.

Third, both f_o and f_i must become asymptotically independent of δ^+. Thus $f_o(\bar{y}, \delta^+) \to f_{o\infty}(\bar{y})$, and $f_i(y^+, \delta^+) \to f_{i\infty}(y^+)$ as $\delta^+ \to \infty$ (otherwise the velocity scales have been incorrectly chosen). This is, in fact, the asymptotic invariance principle.

Now the problem is that in the limit as $\delta^+ \to \infty$, the outer form fails to account for the behaviour close to the wall while the inner fails to describe the behaviour away from it. The question then is: In this limit (as well as for all finite values approaching it) does there exist an 'overlap' region where equation (8.1) is still valid? This question can be answered in the affirmative using the near-asymptotics methodology of George (1995) and GC. The details are the same as for the boundary layer, and are included in Appendix A. To leading order in δ^+, there is, in fact, an overlap region in which

$$\left.\frac{y^+}{f_i}\frac{\partial f_i}{\partial y^+}\right|_{\delta^+} = \gamma(\delta^+) \tag{8.4}$$

and

$$\left.\frac{\bar{y}}{f_o}\frac{\partial f_o}{\partial \bar{y}}\right|_{\delta^+} = \gamma(\delta^+), \tag{8.5}$$

where $\gamma(\delta^+)$ has been defined as

$$\gamma \equiv -\frac{\delta^+}{g}\frac{\mathrm{d}g}{\mathrm{d}\delta^+} = -\frac{\mathrm{d}\ln g}{\mathrm{d}\ln \delta^+}. \tag{8.6}$$

Both equations (8.4) and (8.5) must be invariant to transformations of the form $y \to y + a$ where a is arbitrary (since the equation must be valid for any choice of the origin of y). Therefore, the most general solutions are of the form

$$\frac{U}{U_m} = f_o(\bar{y}, \delta^+) = C_o(\delta^+)[\bar{y} + \bar{a}]^{\gamma(\delta^+)}, \tag{8.7}$$

$$\frac{U}{u_*} = f_i(y^+, \delta^+) = C_i(\delta^+)[y^+ + a^+]^{\gamma(\delta^+)}, \tag{8.8}$$

where the parameters C_o, C_i and γ are functions of δ^+ and must be determined in addition to a. It will be argued later that a^+ is approximately constant. It is interesting to note that the power law form of equations (8.7) and (8.8) was one of those derived by Oberlack (1997) from a Lie group analysis of the equations for parallel shear flows.

It follows immediately from equation (8.1) that the friction law is given by

$$\frac{u_*}{U_m} = g(\delta^+) = \frac{C_o(\delta^+)}{C_i(\delta^+)}\delta^{+-\gamma(\delta^+)}. \tag{8.9}$$

However, equation (8.6) must also be satisfied. Substituting equation (8.9) into equation (8.6) implies that γ, C_o, and C_i are constrained by

$$\ln \delta^+ \frac{\mathrm{d}\gamma}{\mathrm{d}\ln \delta^+} = \frac{\mathrm{d}}{\mathrm{d}\ln \delta^+}\ln\left[\frac{C_o}{C_i}\right]. \tag{8.10}$$

This constraint equation must be invariant to scale transformations of the form $\delta^+ \to D\delta^+$ since the physical choice of $\delta^+ = y^+_{1/2}$ is arbitrary. Thus the Reynolds number dependence of γ and C_o/C_i is independent of the particular choice of $\delta \sim y_{1/2}$ made earlier; any other choice would simply be reflected in the coefficient D. This will be of considerable importance in relating the wall jet parameters to those for the boundary layer obtained earlier by GC. From equation (8.10) we see that both γ and C_o/C_i can be most conveniently expressed as functions of $\ln \delta^+ = \ln D y^+_{1/2}$.

Since by the AIP, equations (8.7) and (8.8) must be asymptotically independent of

Reynolds number, the coefficients and exponent must be asymptotically constant, i.e.

$$\gamma(\delta^+) \to \gamma_\infty,$$
$$C_o(\delta^+) \to C_{o\infty},$$
$$C_i(\delta^+) \to C_{i\infty},$$

as $\delta^+ \to \infty$. Moreover, $C_{o\infty}$ and $C_{i\infty}$ must be non-zero, or else the solutions are trivial. Also, GC have argued that γ_∞ must also be non-zero to ensure a finite local energy dissipation rate at infinite Reynolds number. Therefore none of these three important constants can be zero.

Following GC, it is convenient to write the solution to equation (8.10) as

$$\frac{C_o}{C_i} = \exp\left[(\gamma - \gamma_\infty)\ln\delta^+ + h\right], \tag{8.11}$$

where $h = h(\ln\delta^+)$ remains to be determined, but must satisfy

$$\gamma - \gamma_\infty = -\delta^+\frac{\mathrm{d}h}{\mathrm{d}\delta^+} = -\frac{\mathrm{d}h}{\mathrm{d}\ln\delta^+}. \tag{8.12}$$

The conditions that both $C_{o\infty}$ and $C_{i\infty}$ be finite and non-zero require that:
either

C_o, C_i and γ remain constant always;

or

(i) $\gamma \to \gamma_\infty$ faster than $1/\ln\delta^+ \to 0$

and

(ii) $h(\ln\delta^+) \to h_\infty = \text{constant}$.

It follows immediately that

$$\frac{C_{o\infty}}{C_{i\infty}} = \exp\left[h_\infty\right]. \tag{8.13}$$

Note that condition (i) together with equation (8.12) requires that $\mathrm{d}h/\mathrm{d}\ln\delta^+ \to 0$ faster than $1/\ln\delta^+$. Thus, regardless of the exact functional form of h, the leading term must be $h \sim (\ln\delta^+)^\alpha$ where $\alpha > 0$ to satisfy condition (i).

The behaviour of u_*/U_m obviously is determined by both γ and the ratio C_o/C_i, which are themselves inter-related by equation (8.10). By substituting equations (8.11), (8.12), and (8.13) into equation (8.9), the friction law can be expressed as

$$\frac{u_*}{U_m} = \exp\left[-\gamma_\infty\ln\delta^+ + h\right]. \tag{8.14}$$

Using equation (8.13) this can be re-written as

$$\frac{u_*}{U_m} = \frac{C_{o\infty}}{C_{i\infty}}\delta^{+-\gamma_\infty}\exp\left(h - h_\infty\right). \tag{8.15}$$

Figures 13 and 14 show the mean velocity data in inner and outer variables for three positions of the KEP data ($x/b = 40, 70$, and 100), together with the overlap solutions of equations (8.8) and (8.7) using the h-function of CG and the parameters discussed in § 10 below. Also plotted are two curves described in the following sections used to extend the overlap solution to the wall. The overlap solution provides an excellent fit to the LDA data from approximately $y^+ = 30$ to $\bar{y} = 0.1$. Note that the overlap region is not a straight line on a log-log plot because of the offset parameter a^+ (or $\bar{a}$).

The KEP data for u_*/U_m are plotted in figure 15 as a function of $y^+_{1/2}$. Also shown is equation (8.15), again using the h-function of GC and the parameters given below. The agreement between theory and experiment is excellent.

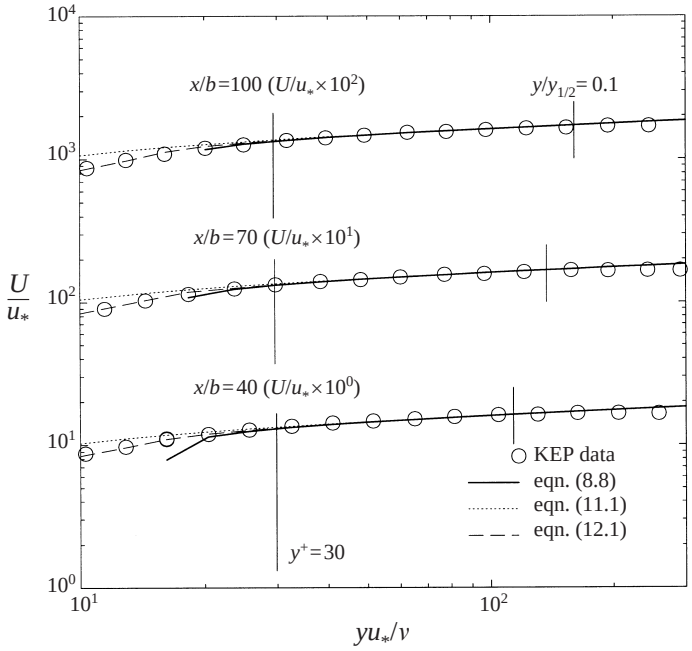

FIGURE 13. KEP data ($x/b = 40, 70$, and 100) and overlap solutions in inner variables.

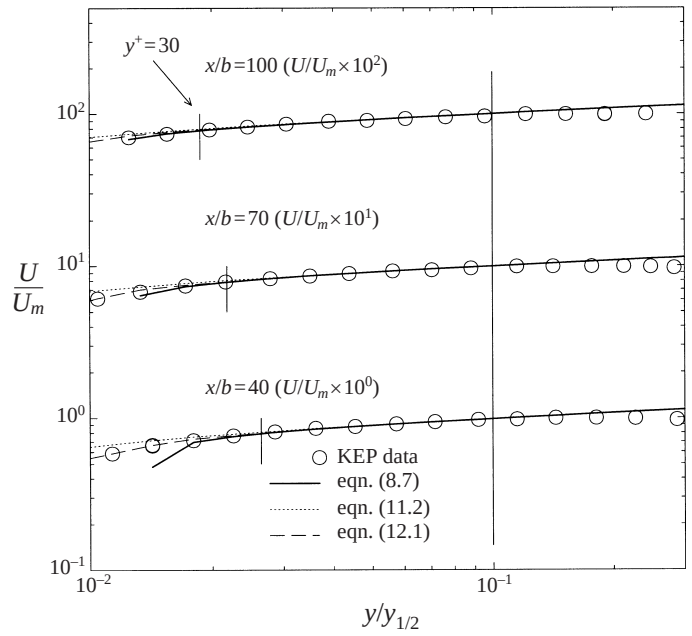

FIGURE 14. KEP data ($x/b = 40, 70$, and 100) and overlap solutions in outer variables.

9. The inertial and mesolayer subregions

The mathematical character of the overlap region has been derived above and is seen to follow directly from first principles without assumptions. It remains to interpret these results physically. The overlap region is essentially the region of the flow where neither convection by the mean motion nor viscous shear stress are of

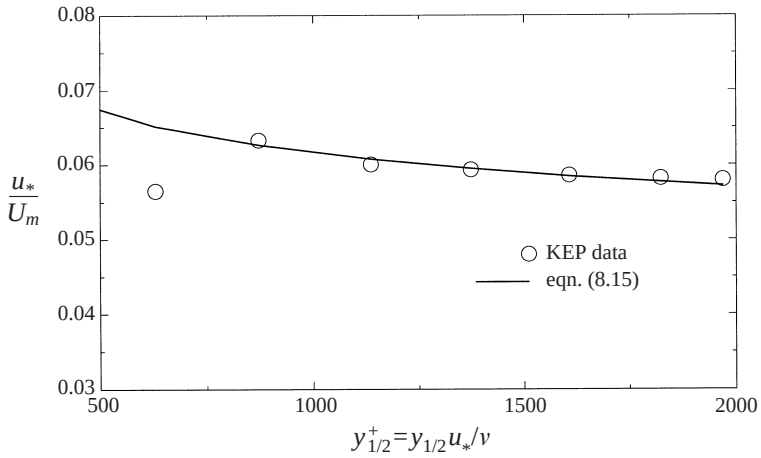

FIGURE 15. u_*/U_m versus $y^+_{1/2}$: KEP data.

major importance in the mean momentum balance. In the wall jet, it is clear from the profiles presented earlier that these conditions are satisfied approximately in the region bounded by $30 < y^+ < 0.1y^+_{1/2}$ (or $30/y^+_{1/2} < \bar{y} < 0.1$), or from just outside the buffer region (where the total stress has evolved from primarily viscous to Reynolds stress only) to just inside the velocity maximum which is near $\bar{y} = 0.17$ as noted earlier. This is illustrated schematically in figure 2. It is important to note that neither mean convection nor viscous effects are completely negligible in the overlap region at finite Reynolds number, and this is the origin of the Reynolds number dependence of the overlap solutions obtained above. In fact, GC have argued using the spectral energy equations that even if viscous effects were small in the single-point equations, they could never be negligible in the two-point equations in the lower part of the overlap region, a subregion which they called the *mesolayer*. Below a value of $y^+ < 300$ approximately, they argued that viscosity directly affects the multi-point Reynolds stress equations, and hence the dissipation and Reynolds stress. Above $y^+ \approx 300$, inertial effects dominate the nonlinear turbulence energy transfer; hence the term *inertial sublayer* is used to describe it.

Thus the overlap region itself has two sublayers within it: the mesolayer and the inertial sublayer. Obviously the latter can exist only when there is a substantial region in the flow satisfying $0.1y^+_{1/2} > 300$ or $y^+_{1/2} > 3000$. Few wall jet experiments satisfy this criterion, and of those, none have been made with techniques which could measure the near-wall region with sufficient accuracy to determine the wall shear stress. In the KEP data, for example, the mesolayer comprises all of the overlap region. Note that this is still substantially better than current DNS capability where even the conditions for a mesolayer are not satisfied, namely $0.1y^+_{1/2} > 30$! In such cases the velocity maximum itself does not even occur in the outer region of the flow, and hence is dependent on flow Reynolds number. Obviously the overlap analysis above should not be expected to apply to such low Reynolds number flows. It is clear then that experiments and/or simulations at much higher Reynolds numbers are necessary before the above theory can be completely tested and the function $h(\ln \delta^+)$ determined beyond doubt.

In spite of the problems presented by the lack of data to test the overlap arguments at sufficiently high Reynolds numbers, equivalent arguments have previously been made for the turbulent boundary layer by GC for which there is at least some data.

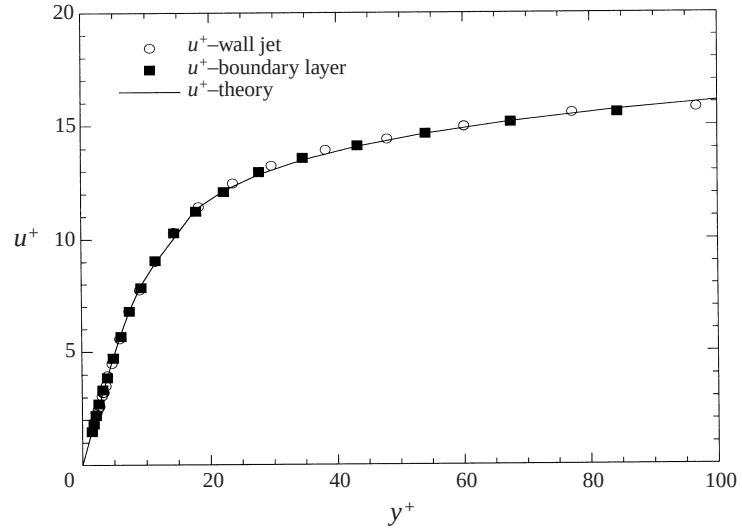

FIGURE 16. Velocity in inner variables for boundary layer and wall jet. Data of Johansson & Karlsson 1989 and KEP, respectively.

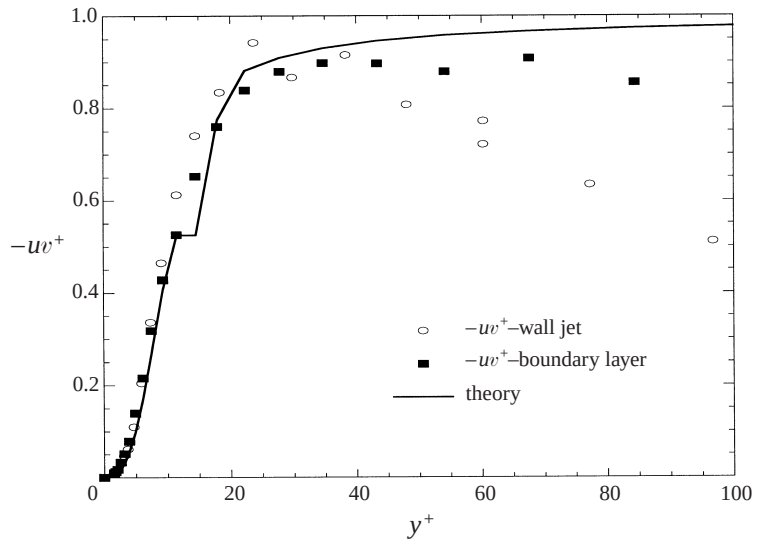

FIGURE 17. Reynolds shear stress in inner variables for boundary layer and wall jet. Data of Johansson & Karlsson 1989 and KEP, respectively.

In fact, the overlap profiles, friction law, and constraint equation for both wall jet and boundary layer are all of the same form. Therefore there is reason to hope that the function $h(\ln \delta^+)$ might be the same for boundary layers and wall jets, at least to within the scale factor D as noted above. These ideas will be formalized and tested below.

10. Wall jet versus boundary layer: a common inner region?

While the outer flows of the zero-pressure-gradient boundary layer and the wall jet are, of course, entirely different, there is reason to suspect that the inner flows

may be the same. First, both scale with the same inner variables, u_* and ν. Second, all the governing equations are exactly the same at infinite Reynolds number, and even the terms which begin to appear at finite Reynolds number are the same. Third, the overlap profiles in inner variables have exactly the same form. Fourth, for both flows the leading term in the Taylor expansion around $y = 0$ is $u^+ = y^+$ and the next non-zero term is the fourth-order term $c_4 y^{+4}$, i.e. $u^+ = y^{++} + c_4 y^{+4} + \cdots$. And finally, as the success of the GC h-function above makes clear, there is experimental evidence. Figures 16 and 17 show the mean velocity and Reynolds stress profiles in inner variables for the Johansson & Karlsson (1989) boundary layer experiment ($R_\theta = 2.4 \times 10^3$) and the KEP wall jet profile for $x/b = 70$ ($y^+_{1/2} = 1.8 \times 10^3$). The mean velocity profiles are nearly identical for $y^+ < 100$, while the Reynolds stress profiles coincide for $y^+ < 35$. Also shown on the figures are the composite velocity given by equation (12.1) and the Reynolds stress profile derived by substituting its derivative into equation (4.9). (The discontinuity arises from the splice described in § 12). These make it clear that the departure of the wall jet profiles from the boundary layer profiles is indeed attributable to the outer flow which penetrates to relatively low values of y^+ at these Reynolds numbers.

Therefore it seems reasonable to hypothesize that:

the inner-variable parameters $C_{i\infty}$, γ_∞, a^+ and c_4 are the same for both the wall jet and the zero-pressure-gradient boundary layer;

the Reynolds number dependence of the parameters C_i and γ is the same, to within the scale factor D discussed in the preceding section.

It follows immediately from equation (8.10) that the outer parameter C_o for the wall jet can at most differ by a constant multiplicative factor from the boundary layer values, since any other difference would change γ. Because this multiplicative factor must also be reflected in $C_{o\infty}$, the only differences between the wall jet and the boundary layer can be $C_{o\infty}$ and the scale factor D; otherwise the second hypothesis is wrong. Finally, the all-important function, $h(\delta^+) - h_\infty$, must be the same for both boundary layers and wall jets, since it determines the Reynolds number behaviour of both γ and C_o/C_i. (Recall that $\delta^+ = Dy^+_{1/2}$.) (Note that a similar line of reasoning was applied by Castillo (1997) to the pressure-gradient boundary layer.)

Thus, as discovered above, the GC empirical form for h for the boundary layer can be incorporated directly here in the form

$$h = \frac{A}{(\ln Dy^+_{1/2})^\alpha}. \tag{10.1}$$

Note that while this may appear to be an arbitrary empirical equation, it is really much more general. Since $h \to h_\infty$ as $\ln Dy^+_{1/2} \to \infty$, only negative powers are possible in an expansion of $h - h_\infty$ for large values, of which equation (10.1) is at least the leading term.

It follows from equations (8.12), (8.11), and (8.15) that

$$\gamma - \gamma_\infty = \frac{\alpha A}{(\ln Dy^+_{1/2})^{1+\alpha}}, \tag{10.2}$$

$$\frac{C_o}{C_i} = \frac{C_{o\infty}}{C_{i\infty}} \exp\left[(1+\alpha)A/(\ln Dy^+_{1/2})^\alpha\right] \tag{10.3}$$

and

$$\frac{u_*}{U_m} = \frac{C_o}{C_i}\left(Dy^+_{1/2}\right)^{-\gamma} = \frac{C_{o\infty}}{C_{i\infty}}[Dy^+_{1/2}]^{-\gamma_\infty} \exp\left[A/(\ln Dy^+_{1/2})^\alpha\right]. \tag{10.4}$$

For the boundary layer, GC found $\alpha = 0.46$, $A = 2.90$, $C_{i\infty} = 55$, $\gamma_\infty = 0.0362$, and $a^+ \approx -16$. If the hypothesis is correct, these values should be the same for the wall jet. Alternatively, if the parameters or the empirical form for h have been more accurately determined for the wall jet, then they should also describe the boundary layer, to within the scale factor D and $C_{o\infty}$ which must be determined for each flow separately. In fact, the CG parameters describe the KEP wall-jet velocity profiles data to within 5% between $y^+ = 30$ and $\bar{y} = 0.1$ using $C_o = C_{o\infty} = 1.26$ and $D = 1.0$. But as illustrated in figures 13 to 15 above, a slight change to $C_o = C_{o\infty} = 1.30$ and $C_{i\infty} = 56.7$ (so $C_{o\infty}/C_{i\infty} = 0.023$ is unchanged) reduces the maximum error in the overlap range of the mean velocity profiles to less than 2%, which is within the experimental uncertainty. Both sets of parameters predict the friction data to within 1% (since u_*/U_m depends only on the ratio of $C_{o\infty}$ to $C_{i\infty}$, and not their individual values). As shown later, a subtle consequence of this will be that all of the differences in spreading rate among the various experiments can be attributed to the parameter B_1 defined in equation (6.2).

11. A mesolayer interpretation of a^+

The a appearing in equations (8.8) and (8.7) has been interpreted by GC as arising from the effect of the turbulence Reynolds number near the wall on the two-point Reynolds stress equations. A useful form of the inner velocity profile can be obtained by expanding the inner velocity profile of equation (8.8) for $y^+ \gg a^+$. The result is

$$\frac{U}{u_*} = C_i y^{+\gamma} + \gamma C_i a^+ y^{+\gamma-1} + \tfrac{1}{2}\gamma(\gamma-1) C_i a^{+2} (y^+)^{\gamma-2} + \cdots. \tag{11.1}$$

Equation (11.1) can also be written in outer variables as

$$\frac{U}{U_m} = C_o \bar{y}^\gamma + \gamma \bar{a} C_o \bar{y}^{\gamma-1} + \tfrac{1}{2}\gamma(\gamma-1) C_o \bar{a}^2 (\bar{y})^{\gamma-2} + \cdots, \tag{11.2}$$

where $\bar{a} = a^+/y^+_{1/2}$.

These forms are useful for two reasons: First, they are excellent approximations to equation (8.8) for all values of $y^+ > -a^+$ (or $\bar{y} > -\bar{a}$). Second, it is easier to incorporate them into a composite solution for the inner region since they do not have the singularity at $y^+ = -a^+$. These profiles have been included on figures 13 and 14 using the GC value of $a^+ = -16$.

12. Composite velocity profiles for the inner and overlap regions

A velocity profile valid over the entire inner and overlap regions can be obtained using equation (11.1) if empirical relations are introduced to account for the variation of $f_i(y^+, \delta^+)$ inside the overlap region. This is analogous to the near-wall and buffer-layer empirical profiles employed by GC for boundary layers which use an empirical relation to splice together the various regions of the flow so that a continuous profile is obtained.

The term 'buffer layer' was used by GC to refer to the region of adjustment from linear to the meso/overlap region. They proposed splicing the near-wall and expanded form of the overlap solutions using

$$\begin{aligned}\frac{U}{u_*} = f_i(y^+) = (y^+ + c_4 y^{+4} + c_5 y^{+5}) \exp(-d y^{+6}) \\ + C_i y^{+\gamma}[1 + \gamma a^+ y^{+-1} + \tfrac{1}{2}\gamma(\gamma-1) a^{+2} y^{+-2}][1 - \exp(-d y^{+6})].\end{aligned} \tag{12.1}$$

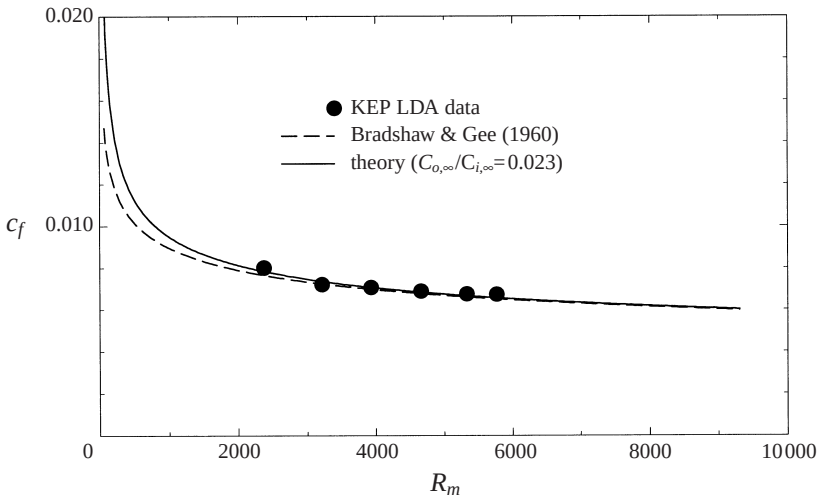

FIGURE 18. Skin friction coefficient versus $R_m = U_m y_m/\nu$.

The y^{+6}-dependence of the exponentials allows not only the no-slip condition to be satisfied at the wall, but also the boundary conditions on the first three velocity derivatives. The damping parameter is chosen as $d = 8 \times 10^{-8}$ to fix the changeover at $y^+ \approx 15$. A constant value of $c_4 = -0.0003$ is in good agreement with both the velocity data of KEP and the corresponding expansion for the Reynolds shear stress near the wall (i.e. $\langle -uv \rangle^+ = 4c_4 y^{+3}$). The value of c_5 cannot be determined with any accuracy from the data, so was arbitrarily chosen as $c_5 = 1.35 \times 10^{-5}$ to provide the best splice between the near-wall and mesolayer profiles. The value of a^+ was determined by GC to be approximately -16.

Figure 16 shows equation (12.1) together with the velocity data in inner variables for the KEP profile ($x/b = 70$) and the boundary layer data of Johansson & Karlsson (1989). Figure 17 shows the corresponding Reynolds stress profile calculated using equation (12.1) and equation (4.9), together with the measured Reynolds stress from these experiments. The calculated profiles use the modified GC values described earlier for the inner parameters ($\gamma_\infty = 0.0362$, $C_{i\infty} = 56.7$, $a^+ = -16$, $\alpha = 0.46$, and $A = 2.9$) with $D = 1.00$ and $C_{o\infty} = 1.30$. The agreement between experiment and theory is remarkable. The slight difference in $C_{i\infty}$ (from the boundary layer value) is undoubtedly attributable to the higher quality of the wall jet data. Overall, the agreement between the composite profile and the velocity data is within 1% for $\bar{y} < 0.1$.

13. The asymptotic friction law

As noted above, it has long been customary to present friction data plotted against the local Reynolds number based on the velocity maximum and half-width (or location of velocity maximum). Such a plot is not naturally suggested by the theory presented here since the parameters depend on $y^+_{1/2}$, and not on $U_m y_{1/2}/\nu$ or $U_m y_m/\nu$. It can easily be generated on a spreadsheet, however, by assuming a value for $y^+_{1/2}$, then calculating u_*/U_m and from the two, R_m. To facilitate comparison with earlier empirical friction laws and data, such a plot is presented here as figure 18, where it has again been assumed that $y_m/y_{1/2} = 0.17$. Representative values are shown in table 1.

$y^+_{1/2}$ (given)	C_o ($\approx C_{o\infty}$)	C_i (eqn. (10.3))	γ (eqn. (10.2))	u_*/U_m (eqn. (8.9) or (10.4))	$R_m = y_m U_m/\nu$ ($y_m/y_{1/2} = 0.17$)
1000	1.3	9.53	0.1151	0.0616	2758
1500	1.3	9.95	0.1089	0.0589	4329
2000	1.3	10.25	0.1050	0.0571	5952
3000	1.3	10.65	0.1000	0.0548	9307
5000	1.3	11.14	0.0946	0.0521	16301
7000	1.3	11.45	0.0914	0.0505	23547
10000	1.3	11.77	0.0884	0.0489	34734

TABLE 1. Wall jet parameters calculated as a function of $y^+_{1/2}$.

Since there is no new information, it is not surprising that the same good agreement noted above is achieved. Also shown is the Bradshaw & Gee (1960) correlation. This was originally given by the authors in terms of c_f as a power law in $R_m \equiv U_m y_m/\nu$; in particular, $c_f = 0.0315 R_m^{-0.182}$. This transforms to $u_*/U_m = 0.122(y^+_{1/2})^{-0.100}$ using the KEP estimate of $y_m/y_{1/2} = 0.17$. There is a remarkable correspondence between the theoretical curve and the empirical relation of Bradshaw & Gee (1960). The theoretical and empirical curves diverge as the Reynolds number increases since the power exponent continues to drop in the former, but is fixed in the latter. Obviously the empirical expressions should not be used outside the limited range for which they were established by experiment, but the theory is not so limited.

As shown in equation (10.4), u_*/U_m is entirely determined by the two constants, γ_∞ and $C_{o\infty}/C_{i\infty}$, and the function $h(Dy^+_{1/2})$. In the limit of infinite Reynolds number, however, even the function h must be constant, so the asymptotic friction law is indeed a power law with constant coefficients, i.e.

$$\frac{u_*}{U_m} \to \frac{C_{o\infty}}{C_{i\infty}}(Dy^+_{1/2})^{-\gamma_\infty}. \tag{13.1}$$

Some idea of when this limiting power law is valid can be obtained by expanding the exponential of equation (10.4) in powers of $A/(\ln(Dy^+_{1/2})^\alpha$:

$$\exp\left[A/(\ln Dy^+_{1/2})^\alpha\right] = 1 + \frac{A}{(\ln Dy^+_{1/2})^\alpha} + \cdots. \tag{13.2}$$

Clearly the second term must be negligible for the power law limiting behaviour to dominate; thus the limiting power law behaviour is obtained when

$$\ln Dy^+_{1/2} \gg [A]^{1/\alpha}. \tag{13.3}$$

For the values above this would require $y^+_{1/2} \gg 2.4 \times 10^4$, which is an order of magnitude above the existing experiments.

14. Implications for $y_{1/2}$ and U_m versus x

Figures 19–22 show the variation of the half-width, $y_{1/2}$, and the velocity maximum, U_m, with downstream distance, x, for the KEP, AJL and WKH data. These data are plotted using both the traditional normalization using b and U_o (cf. Launder & Rodi 1981), and using M_o and ν (cf. Narasimha *et al.* 1973; WKH). Also shown for the latter are the theoretical curves derived below.

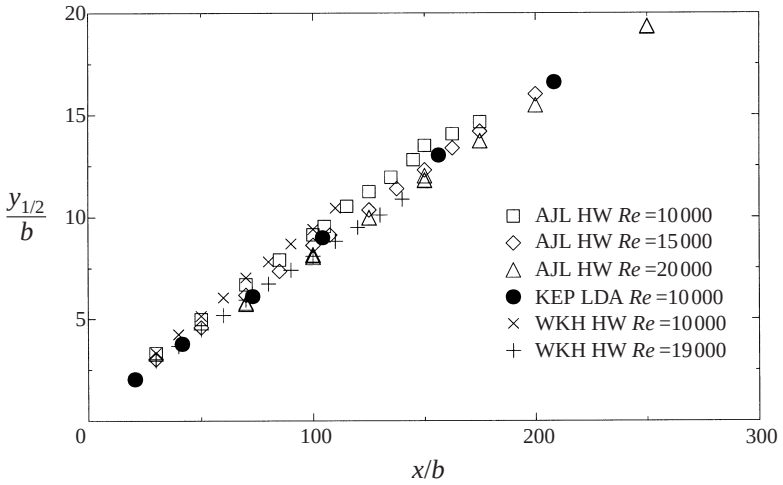

FIGURE 19. Variation of half-width with downstream distance, $y_{1/2}/b$ versus x/b: KEP, AJL and WKH data.

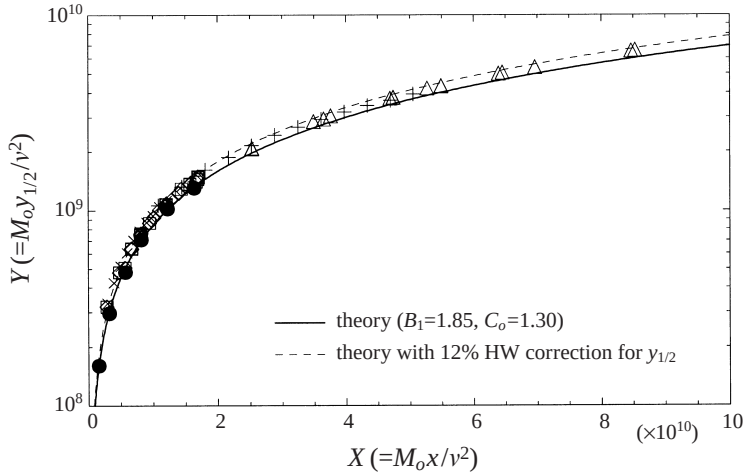

FIGURE 20. $Y = M_o y_{1/2}/\nu^2$ versus $X = M_o x/\nu^2$: KEP, AJL and WKH data; symbols as figure 19.

It is not entirely clear whether the data collapse or not even when plotted using the momentum/viscosity scaling (which is seen to work somewhat better than the scaling using U_m and b). The same lack of collapse was observed by WKH who attempted to remove the trends with a virtual origin, with limited success. These differences between data sets were noted in § 6 in the normalized plots of U_m versus $y_{1/2}$. Clearly source Reynolds number alone cannot explain the differences since the WKH source Reynolds numbers overlap those of AJL and KEP. As noted earlier there is nothing in the single-point similarity equations themselves to suggest that the effect of initial conditions dies off. It is precisely here in B_1, $\mathrm{d}y_{1/2}/\mathrm{d}x$ and $\mathrm{d}U_m/\mathrm{d}x$ where the differences appear. Nonetheless, the cross-flow and rectification errors in the hot-wire measurements due to the turbulence intensity at least account for some of the observed differences. All of the hot-wire estimates of $y_{1/2}$ are about 10% to 15% higher than the LDA and theoretical results, consistent with the error estimate of

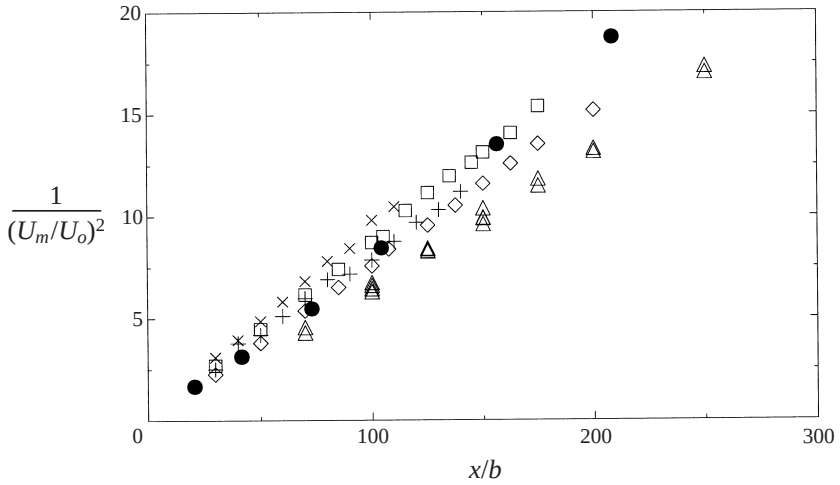

FIGURE 21. Variation of centreline velocity with distance, $1/(U/U_o)^2$ versus x/b: KEP, AJL and WKH data; symbols as figure 19.

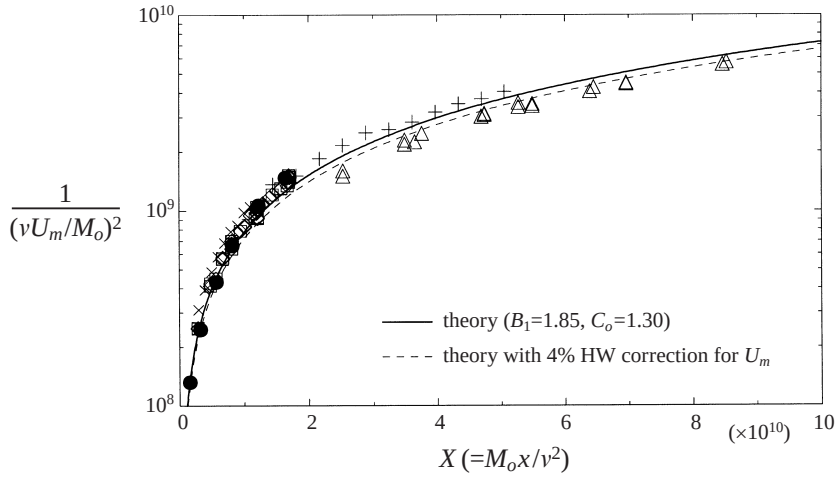

FIGURE 22. $1/(vU_m/v)^2$ versus $X = M_o x/v^2$: KEP, AJL and WKH data; symbols as figure 19.

EKP. Near the velocity maximum, the hot-wire-obtained mean velocity measurement are 3% to 5% too high, which means that the plotted hot-wire data in figure 22 should be 6% to 10% too low. This is at least in the correct direction for the AJL data, but cannot account for the WKH data. As noted in § 6, however, we might have overestimated the WKH values of M_o by about the same amount which would have the opposite effect. So the role of the initial conditions, if any, must remain unresolved for now.

It has regularly been conjectured (e.g. Launder & Rodi 1981) that the half-width of the plane wall jet grows linearly with distance. It will be argued below that $\mathrm{d}y_{1/2}/\mathrm{d}x$ is proportional to the shear stress, and it has already been shown that the only possible asymptotic limit for this is zero. However, $\mathrm{d}y_{1/2}/\mathrm{d}x \to 0$ does not imply that the wall jet stops growing, only that it cannot grow faster than linear. For example, if $\mathrm{d}y_{1/2}/\mathrm{d}x \sim x^p$ where $0 > p > -1$, then clearly $\mathrm{d}y_{1/2}/\mathrm{d}x \to 0$ as $x \to \infty$, but

$y_{1/2} = x^{1+p}/(1+p)$ continues to increase. The growth is not linear, however, unless $p \equiv 0$, which we shall see it is not. In fact, most experiments which have attempted to establish empirical power laws for the x-dependence of the half-width conclude that the growth rate is slightly less than linear. For example, WKH and Narasimha *et al.* (1973) suggest on empirical grounds that $y_{1/2} \sim (x - x_o)^{0.88}$ and $y_{1/2} \sim (x - x_o)^{0.91}$, respectively. As will be shown below, there is no theoretical justification for such power laws in x except for very large values of the Reynolds number, and well above any experiments to-date.

The x-dependence of $y_{1/2}$ can be considered using the momentum integral equation in outer similarity variables, which can be written as

$$U_m^{-2} \frac{\mathrm{d}}{\mathrm{d}x} \left[U_m^2 y_{1/2} I_2 \right] = -\frac{u_*^2}{U_m^2}, \tag{14.1}$$

where I_2 is defined by

$$I_2 = \int_0^\infty [f_o^2 + 2(k_u - k_v)] \mathrm{d}\bar{y}. \tag{14.2}$$

The turbulence normal stress term, $(k_u - k_v)$ is of second order, and could have been omitted with no loss of generality but an error of approximately 5% would be introduced. Note that I_2 becomes asymptotically independent of the Reynolds number in the limit as $y_{1/2}^+ \to \infty$.

The similarity condition of equation (5.7) (i.e. $U_m \sim y_{1/2}^n$) implies that

$$\frac{y_{1/2}}{U_m} \frac{\mathrm{d}U_m}{\mathrm{d}x} = n \frac{\mathrm{d}y_{1/2}}{\mathrm{d}x}. \tag{14.3}$$

It follows after some manipulation that

$$\left\{ (1+2n) I_2 + \frac{\mathrm{d}I_2}{\mathrm{d} \ln y_{1/2}^+} \right\} \left[\frac{\mathrm{d}y_{1/2}}{\mathrm{d}x} \right] = -\frac{u_*^2}{U_m^2}. \tag{14.4}$$

In the limit as $y_{1/2}^+ \to \infty$, this reduces to

$$(1+2n) I_2 \left[\frac{\mathrm{d}y_{1/2}}{\mathrm{d}x} \right] = -\frac{u_*^2}{U_m^2}. \tag{14.5}$$

Note the appearance of the exponent n from the similarity condition of equation (5.7).

The value $n = -1/2$ is a special case since the corresponding shear stress must be zero, and hence the growth rate either becomes undefined or must be exactly zero. In fact, from equation (5.7) it is clear that $n = -1/2$ would require that that $U_m^2 y_{1/2}$ be constant, which is exactly the momentum conservation condition for a free plane jet (cf. George 1995), and this makes sense only if there is no momentum loss to the boundary. Given the presence of the wall, this would be a possibility only at infinite source Reynolds number, if at all. For finite source Reynolds numbers, the presence of the wall dictates a continuing momentum loss to the wall so that $n < -1/2$, and as a consequence $y_{1/2}$ must grow slower than linearly with x, exactly as suggested by Narasimha *et al.* (1973) , WKH and AJL on empirical grounds. But there is, to this point at least, nothing in the equations to indicate that the value of n is universal, although the experiments cited earlier in § 6 suggest that it might be.

The derivative, $\mathrm{d}y_{1/2}/\mathrm{d}x$, in equation (14.5) can be replaced by either $\mathrm{d}(y_{1/2}/b)/\mathrm{d}(x/b)$ or $\mathrm{d}Y_{1/2}/\mathrm{d}X$ with no loss of generality, where $Y_{1/2}$ is defined as before and X

$y^+_{1/2}$ (given)	$\mathrm{d}y_{1/2}/\mathrm{d}x$ (eqn. (14.5))	$X = M_o x/\nu^2$ (eqn. (14.9))	$Y = M_o y_{1/2}/\nu^2$ (eqn. (14.6))	$1/(\nu U_m/M_o)^2$ (eqn. (6.2))
1000	0.0870	2.35E+09	2.26E+08	1.94E+08
1500	0.0794	6.72E+09	5.87E+08	5.31E+08
2000	0.0747	1.41E+10	1.15E+09	1.08E+09
3000	0.0687	3.96E+10	2.97E+09	2.94E+09
5000	0.0622	1.44E+11	9.74E+09	1.03E+10
7000	0.0585	3.35E+11	2.12E+10	2.35E+10
10 000	0.0548	8.17E+11	4.84E+10	5.61E+10

TABLE 2. Wall jet development as a function of $y^+_{1/2}$. (See table 1 for parameters.)

by $X \equiv xM_o/\nu^2$. The momentum–viscosity scaled version is used below to derive the X-dependence of $Y_{1/2}$ and $\nu U_m/M_o$.

Since n, I_2 and u_*/U_m can be determined directly from the data, equation (14.5) can be used to calculate $\mathrm{d}y_{1/2}/\mathrm{d}x$. Alternatively, n can be determined if I_2, u_*/U_m, and $\mathrm{d}y_{1/2}/\mathrm{d}x$ are known. In fact, this is probably the best way to determine n since $2n$ is very close to -1, so the difference between n and $-1/2$ is magnified. The value so obtained can then be used together with the continuity equation developed in the next section to provide an overall consistency check on the flow and data. From the KEP data, the value of I_2 for $x/b = 40$, 70, 100 (and even 150) is 0.78 (0.745 if the turbulence terms are neglected). Using this, the measured values of u_*/U_m and $\mathrm{d}y_{1/2}/\mathrm{d}x$, and averaging the result yields $n = -0.528$, which is the value cited earlier in § 5.

Since the values of n and I_2 can now be assumed known, then the x-dependence of $Y_{1/2}$ (or $y_{1/2}/b$) can be calculated numerically using equation (14.5) together with the friction law of equation (10.4). The local value of $y^+_{1/2}$ must be determined for each value of x before the integration can be performed, so an inverse procedure was carried out using a spreadsheet, the results of which are summarized in table 2. It follows after some manipulation that

$$\frac{M_o y_{1/2}}{\nu^2} = Y_{1/2} = \left[\frac{1}{B_1}\left(\frac{C_i D^\gamma}{C_o}\right)\right]^{1/(1+n)} [y^+_{1/2}]^{(1+\gamma)/(1+n)} \tag{14.6}$$

so $Y_{1/2}$ can be obtained directly for each selected value of $y^+_{1/2}$. Moreover, from equations (14.5), (10.4), and (6.2) it can also be shown that

$$\frac{\mathrm{d}Y_{1/2}}{\mathrm{d}X} = \left[\frac{-1}{(1+2n)I_2}\right]\left(\frac{C_o}{C_i}\right)^{2/(1+\gamma)} [DB_1 Y_{1/2}^{(1+n)}]^{-2\gamma/(1+\gamma)}. \tag{14.7}$$

Note especially the appearance of B_1 in equation (14.7). This is the only way for the source dependence of $y_{1/2}$ and U_m to influence the growth rate calculation if n is assumed universal. As noted in § 6, it is not at all clear whether B_1 is universal.

A finite difference estimate of $\mathrm{d}Y_{1/2}/\mathrm{d}X$ is given by

$$\frac{\mathrm{d}Y_{1/2}(X)}{\mathrm{d}X} \approx \frac{Y_{1/2}(X+\Delta X) - Y_{1/2}(X)}{\Delta X}. \tag{14.8}$$

From this $X - X_o$ can be readily obtained by summing the ΔX estimated from

$$\Delta X = \frac{Y_{1/2}(X+\Delta X) - Y_{1/2}(X)}{\mathrm{d}Y_{1/2}/\mathrm{d}X}, \tag{14.9}$$

where for each incremental increase in the value of $y^+_{1/2}$ from a small value, the values of $Y_{1/2}$ are obtained from equation (14.6) and $\mathrm{d}Y_{1/2}/\mathrm{d}X$ from equation (14.8). Note that X_o is a possible virtual origin chosen to be zero for the computations shown in figure 20 and table 2. The results shown were obtained by starting at $y^+_{1/2} = 40$ and using increments of $\Delta y^+_{1/2} = 10$.

Figure 20 shows the calculated variation of $Y_{1/2}$ versus X for the using the values of $B_1 = 1.85$ and $n = -0.528$ determined in § 6. Also shown are the KEP, AJL and WKH data. There is excellent agreement between data and theory, especially if the errors for hot-wires in high intensity turbulence are taken into account. It is straightforward to convert this $Y_{1/2}$ versus X information to $y_{1/2}/b$ versus x/b using equation (6.3) and the definitions of $Y_{1/2}$ and X, at least for a top-hat profile source, but the results depend B_1 and source Reynolds number as noted in § 6.

The velocity maxima can readily be calculated as a function of x once the x-variation of $y_{1/2}$ is known using equation (6.2). The calculated results using $B_1 = 1.85$ are shown in figure 22, along with the experimental data of KEP, AJL and WKH. The experiments and theory are in reasonable agreement. Note that the agreement for each individual data set is considerably improved if the optimum values of B_1 for each data set are used. As noted above, the uncertainty of the hot-wire data does not seem to warrant this tinkering.

As noted above, it has long been customary to fit power laws to wall jet data. In fact, power law expressions for $y_{1/2}$ and U_m as functions of x can be obtained by assuming the parameters C_i, C_o and γ to be locally constant. These, of course, are not valid for the entire range of x, but are useful in understanding such fits from earlier experiments. If this assumption is made, then the dependence of C_i, C_o and γ on y^+ can be ignored, and equation (14.7) can be integrated directly to yield

$$Y_{1/2} = B_{2,local}(X - X_o)^{(1+\gamma)/(1+3\gamma+2n\gamma)}, \tag{14.10}$$

where

$$B_{2,local} \equiv \left\{ \frac{-(1+3\gamma+2n\gamma)}{(1+\gamma)(1+2n)I_2} \left(\frac{C_o}{C_i}\right)^{2/(1+\gamma)} (DB_1)^{-2\gamma/(1+\gamma)} \right\}^{(1+\gamma)/(1+3\gamma+2n\gamma)} \tag{14.11}$$

and X_o is a virtual origin which depends on the Reynolds number range under consideration. Note that there would be an additional Reynolds number dependence in the coefficient if $y_{1/2}/b$ and x/b had been used instead of $Y_{1/2}$ and X.

If the parameters are evaluated at $y^+_{1/2} = 1500$ (which corresponds approximately to the KEP experiment at $x/b = 100$), then $C_o/C_i = 0.12$, and $\gamma = 0.109$. Thus locally, $Y_{1/2} = 0.515(X - X_o)^{0.915}$. This exponent is exactly that obtained by AJL, and very much in the range observed by WKH and Narasimha *et al.* (1973). The coefficient is quite different, however, indicating that the virtual origin must be quite large and negative, in fact nearly as large as x/b itself to achieve estimates in reasonable agreement with the data. The fact that these are only local estimates means that the power will increase as higher local Reynolds numbers are achieved, as will the magnitude of the virtual origin required. Recall that no virtual origin at all was required in the numerical integration above which made no assumptions about the constancy of the parameters, but evaluated them at each step in the integration.

Finally, it is easy to show that the true asymptotic behaviour is indeed a power law. Like the friction law, however, this asymptotic will be achieved at Reynolds numbers far above those of current experiments. In the limit as $y^+_{1/2} \to \infty$, all the parameters

are exactly constant, so in this limit equation (14.11) represents the exact asymptotic variation of $Y_{1/2}$. Using $n = -0.528$, $I_2 = 0.78$, $\gamma_\infty = 0.0362$, $C_{o\infty}/C_{i\infty} = 0.023$ and $B_1 = 1.85$ yields $B_{2\infty} = 0.019$ and the exponent is 0.97. Thus the asymptotic variation of $Y_{1/2}$ with X is nearly linear, but not quite. The difference from linear behaviour is quite important, however, since as shown above it is a consequence of the continuing momentum loss to the wall. And even this relation depends on the value of B_1, and hence perhaps the source conditions. Note that this limiting power law growth rate cannot be achieved until the friction law has achieved its asymptotic power law, namely when the inequality of equation (13.3) is satisfied.

15. Implications of the continuity equation

The averaged continuity equation can be integrated from the wall to y to obtain

$$V = -\int_0^y \frac{\partial U}{\partial x}\mathrm{d}y'. \tag{15.1}$$

It follows immediately that

$$V_\infty = -\int_0^\infty \frac{\partial U}{\partial x}\mathrm{d}y'. \tag{15.2}$$

Obviously any attempt to realize a plane wall jet must satisfy these equations. In general they are difficult to apply, however, because of the x-derivatives. As will be shown below, similarity simplifies this process considerably so that continuity can be used both to verify the two-dimensionality of the flow and to provide further evidence that the flow is indeed similar and the measurements of it are correct.

The outer-variables version of the continuity equation can be easily derived by substituting equation (5.11) to obtain

$$\frac{V}{U_m} = \left[\frac{\mathrm{d}y_{1/2}}{\mathrm{d}x}\right]\bar{y}f_o(\bar{y}, y^+_{1/2}) - \left[\frac{y_{1/2}}{U_m}\frac{\mathrm{d}U_m}{\mathrm{d}x} + \frac{\mathrm{d}y_{1/2}}{\mathrm{d}x}\right]\int_0^{\bar{y}} f_o(\xi, y^+_{1/2})\mathrm{d}\xi$$
$$- \left[y_{1/2}\frac{\mathrm{d}y^+_{1/2}}{\mathrm{d}x}\right]\frac{\partial}{\partial y^+_{1/2}}\int_0^{\bar{y}} f_o(\xi, y^+_{1/2})\mathrm{d}\xi. \tag{15.3}$$

Note that this equation is valid for all values of $\bar{y}$ as long as $y^+_{1/2}$ is finite.

Since f_o is a similarity solution of the outer equations as $y^+_{1/2} \to \infty$ (i.e. $f_o \to f_{o\infty}$) the last integral is Reynolds number independent in the limit; hence the last term vanishes in the limit. Thus in the limit, the velocity profile in the outer region of the flow must satisfy

$$\frac{V}{U_m}\left[\frac{\mathrm{d}y_{1/2}}{\mathrm{d}x}\right]^{-1} = \bar{y}f_{o\infty}(\bar{y}) - (1+n)\int_0^{\bar{y}} f_{o\infty}(\xi)\mathrm{d}\xi, \tag{15.4}$$

where equation (14.3) has been to used to relate $\mathrm{d}U_m/\mathrm{d}x$ to $\mathrm{d}y_{1/2}/\mathrm{d}x$. It follows immediately that in the same limit, the entrainment velocity is given by

$$\frac{V_\infty}{U_m} = -(1+n)I_1\left[\frac{\mathrm{d}y_{1/2}}{\mathrm{d}x}\right] \tag{15.5}$$

where

$$I_1 \equiv \int_0^\infty f_{o\infty}(\xi)\mathrm{d}\xi. \tag{15.6}$$

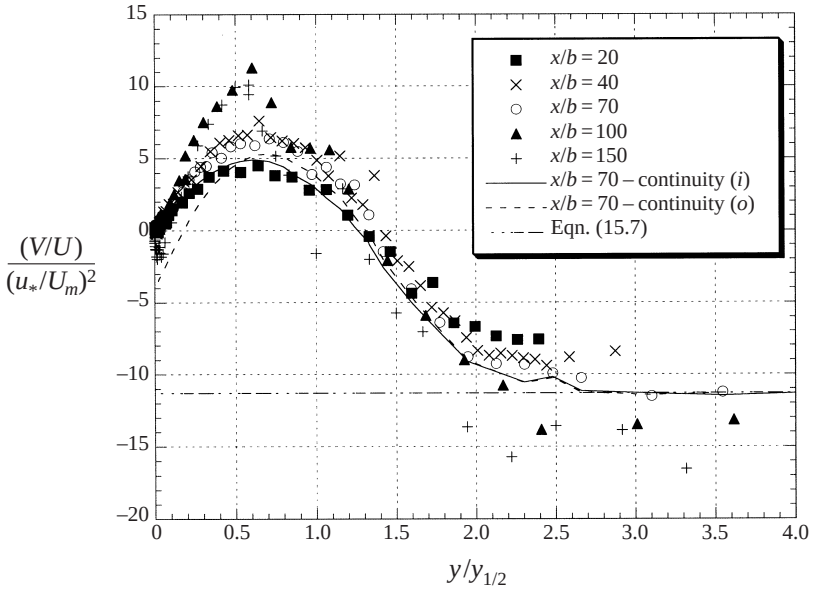

FIGURE 23. Profiles of $V/U_m/(u_*^2/U_m^2)$; KEP data, theory: $n = -0.528$, $I_1 = 1.05$.

Note that since from equation (14.5) $\mathrm{d}y_{1/2}/\mathrm{d}x$ depends on $y_{1/2}^+$, so does V_∞/U_m. On the other hand, if the value of n (and hence the corresponding mean velocity profiles) are universal, then the ratio $(V_\infty/U_m)/[\mathrm{d}y_{1/2}/\mathrm{d}x]$ must be a universal constant.

The integral, I_1, in equation (15.6) was estimated from the KEP data by averaging the integral of U/U_m for $x/b = 40, 70$, and 100; the result was $I_1 \approx 1.05$ to within 2%. The value of $n = -0.528$ was obtained using the integral momentum equation as described in § 14 above. Using these, the calculated value of $(V_\infty/U_m)/[\mathrm{d}y_{1/2}/\mathrm{d}x]$ for the KEP data is 0.50. This can be compared to the ratios inferred from the measurements using the local estimates of V_∞/U_m and $\mathrm{d}y_{1/2}/\mathrm{d}x$ which were $-0.47, -0.48, -0.55$, and -0.71 for positions $x/b = 40, 70, 100$, and 150 respectively. Clearly the value for $x/b = 150$ differs substantially from the rest, but so does the value of I_1 there which increases to 1.10. Both of these are clear indicators that similarity is breaking down because of either a lack of two-dimensionality, or a return flow, or both.

If the flow satisfies the similarity conditions, then the profile of V/U_m in the outer region should collapse when normalized by either $\mathrm{d}y_{1/2}/\mathrm{d}x$ or u_*^2/U_m^2. In the KEP experiment the latter are determined with more accuracy than the former because of the excellent resolution of the measurements near the wall. Figure 23 shows the actual profiles of $(V/U_m)/(u_*^2/U_m^2)$. Also shown are the profiles calculated from equation (15.4) using the values of n and I_1 cited above, and from integrating the U/U_m profile for the $x/b = 70$ position. The agreement between the measured and calculated peak values is within 10% for $x/b = 40, 70$ and 100, but the relative error increases to nearly 30% for $x/b = 150$. Also shown on the plot as a horizontal dashed line is the theoretical limiting value given by

$$\frac{V_\infty/U_m}{u_*^2/U_m^2} = \frac{(1+n)I_1}{(1+2n)I_2}. \tag{15.7}$$

Using the values cited above yields $(V_\infty/U_m)/(u_*^2/U_m^2) = -11.3$ (which corresponds to the value estimated above of $(V_\infty/U_m)/[\mathrm{d}y_{1/2}/\mathrm{d}x] = -0.50$).

The discrepancy between the measured and calculated profiles at $y/b = 40$ can in part be attributed to the Reynolds number dependent terms in equation (15.4) which are not yet negligible since the flow is still developing. Such is not the case beyond $x/b = 100$ where the outermost data show substantial development with distance, thus providing additional evidence that the return flow in the facility is beginning to affect the wall jet part of the flow as noted above.

Another part of the discrepancies must be attributed to measurement errors. EKP have noted that since the values of V are very small compared to U, a very tiny error in the angle between the beams of an LDA system can make a large error in the determination of V. For example, a change in the beam angle of only 0.3° makes about a 10% difference in the V-profiles. Therefore, in cases where similarity behaviour has been established using the U-velocity profile, the V-profiles calculated from similarity may be considered more accurate than those measured. This is a wonderful example of how the theory can be used to refine the measurement parameters, as long as both two-dimensionality and similarity have been established.

The inner part of the wall jet can also be considered by using the inner scaled profile of equation (4.10). It is straightforward to show that

$$\frac{V}{u_*} = -\left[\frac{\eta}{u_*}\frac{\mathrm{d}u_*}{\mathrm{d}x}\right] y^+ f_i(y^+) - \eta \frac{\mathrm{d}y^+_{1/2}}{\mathrm{d}x}\frac{\mathrm{d}}{\mathrm{d}y^+_{1/2}}\int_0^{y^+} f_i(\xi, y^+_{1/2})\mathrm{d}\xi. \tag{15.8}$$

In the limit as $y^+_{1/2} \to \infty$ this reduces to

$$\frac{V}{u_*} = -\left[\frac{\eta}{u_*}\frac{\mathrm{d}u_*}{\mathrm{d}x}\right] y^+ f_i(y^+). \tag{15.9}$$

It is easy to show from a Taylor expansion and the inner momentum equation that the velocity very near the wall is given by $u^+ = y^+ + c_4 y^{+4} + \cdots$ and $v^+ = e_2 y^{+2} + e_3 y^{+3} + \cdots$ (see Monin & Yaglom 1971). It follows immediately from equation (15.9) that

$$v^+ = -\left[\frac{\eta}{u_*}\frac{\mathrm{d}u_*}{\mathrm{d}x}\right][y^{+2} + c_4 y^{+5} + \cdots]. \tag{15.10}$$

Thus $e_2 = [(\eta/u_*)/(\mathrm{d}u_*/\mathrm{d}x)]$, $e_3 = e_4 = 0$ and $e_5 = c_4[(\eta/u_*)/(\mathrm{d}u_*/\mathrm{d}x)]$. Interestingly, e_2 and e_5 are Reynolds number dependent, contrary to the usual assumptions that they are constant.

By using the friction law derived, equation (10.4), together with the similarity condition of equation (5.7), it can be shown after some manipulation that

$$\frac{\eta}{u_*}\frac{\mathrm{d}u_*}{\mathrm{d}x} = \left[\frac{n-\gamma}{1+\gamma}\right]\frac{1}{y^+_{1/2}}\frac{\mathrm{d}y_{1/2}}{\mathrm{d}x} \tag{15.11}$$

or using equation (14.5)

$$\frac{\eta}{u_*}\frac{\mathrm{d}u_*}{\mathrm{d}x} = -\left[\frac{n-\gamma}{1+\gamma}\right]\left[\frac{1}{(1+2n)I_2 y^+_{1/2}}\right]\left(\frac{u_*}{U_m}\right)^2. \tag{15.12}$$

Given the experimental difficulties in obtaining mean V-velocity data so close to the wall (both because of its very small magnitude and the proximity of the wall), the velocity calculated from equations (15.9) using (15.12) is probably the only way V can be obtained here. This is an excellent example of how theory can be used to obtain indirectly a result which is not measurable at all.

16. Summary and conclusions

A new theory has been set forth based on the asymptotic invariance principle in which the outer wall jet is governed by different scaling parameters than commonly believed. In particular, the Reynolds shear stress in the outer layer scales to first order with u_*^2, so that the outer layer is governed by two velocity scales, U_m and u_*. Both inner and outer regions become asymptotically independent of the Reynolds number, and reduce to similarity solutions of the inner and outer boundary layer equations in the limit of infinite Reynolds number. A consequence of this is that no scaling laws can perfectly collapse the data at finite Reynolds number.

By examining the inner and outer velocity profiles using near-asymptotics, the velocity in the overlap layer was shown to exhibit power law behaviour, but with an exponent which was only asymptotically constant. This overlap region is not Reynolds number invariant in either inner or outer variables, contrary to common belief, but consistent with recent experimental findings. Another consequence of the analysis was that the friction coefficient varied as a power of the local Reynolds number, the power and coefficients being entirely determined by the velocity parameters, or vice versa. New scaling laws for the turbulence quantities in the outer layer were also derived from similarity considerations of the turbulence Reynolds stress equations. The theory was shown to be in excellent agreement with the all the experimental data. In addition, the hypothesis that the inner flow of the zero-pressure-gradient boundary layer and the wall jet are the same appears to be supported.

At the very least, a strong motivation has been provided for a careful re-analysis of the older experiments, and perhaps a new generation of experiments over the entire range of Reynolds numbers. Of particular interest will be determining whether there are features of the initial conditions which are preserved, and what exactly are the asymptotic values of the parameters. The success of the theory in correlating the observations to-date, all of which were made before the theory was deduced, lends considerable credibility to the AIP approach to similarity.

The authors are grateful to L. Castillo, J. Citriniti, D. Ewing, B. Johansson, and J. Persson for their assistance and helpful comments during the course of this work. They are also grateful to Chalmers University of Technology and Vattenfall Utveckling AB for their support for this cooperative effort, without which this work would have been impossible. The assistance of I. Wygnanski and M. Zhou of the University of Arizona in accessing and understanding the WKH data was very much appreciated. W.K.G. would like to also express his gratitude to the former for his suggestion at IIT in January 1995 that the wall jet might be an interesting application of the AIP approach.

Appendix A. Details of the overlap analysis

The methodology used to determine the overlap characteristics was introduced by George (1995) and was termed 'near-asymptotics'. It is necessary because the traditional approaches to asymptotic matching cannot account for the possibility of a power exponent tending to zero, which cannot be ruled out without additional arguments. This Appendix has been adapted from the GC paper, and is included here for completeness.

The question of whether there is a common region of validity can be investigated by examining how rapidly f_o and f_i are changing with δ^+. From the Taylor expansion

of the velocity derivatives in equation (8.3) about a fixed value of δ^+,

$$\frac{f_i(y^+;\delta^+ + \Delta\delta^+) - f_i(y^+;\delta^+)}{\Delta\delta^+ f_i(y^+;\delta^+)} \approx \frac{1}{f_i(y^+;\delta^+)} \frac{\partial f_i(y^+;\delta^+)}{\partial \delta^+}\bigg|_{y^+} \equiv S_i(\delta^+, y^+) \tag{A 1}$$

and

$$\frac{f_o(\bar{y};\delta^+ + \Delta\delta^+) - f_o(\bar{y};\delta^+)}{\Delta\delta^+ f_o(\bar{y};\delta^+)} \approx \frac{1}{f_o(\bar{y};\delta^+)} \frac{\partial f_o(\bar{y};\delta^+)}{\partial \delta^+}\bigg|_{\bar{y}} \equiv S_o(\delta^+, \bar{y}). \tag{A 2}$$

Thus S_i and S_o are measures of the Reynolds number dependences of f_i and f_o respectively. Both vanish identically in the limit as $\delta^+ \to \infty$. If y^+_{max} denotes a location where outer flow effects begin to be strongly felt on the inner scaled profile, then for $y^+ < y^+_{max}$, S_i should be much less than unity (or else the inner scaling is not very useful). Similarly, if $\bar{y}_{min}$ measures the location where viscous effects begin to be strongly felt (e.g. as the linear velocity region near the wall is approached), then S_o should be small for $\bar{y} > \bar{y}_{min}$. Obviously either S_i or S_o should increase as these limits are approached. Outside these limits, one or the other should increase dramatically.

The quantities S_i and S_o can, in fact, be used to provide a formal definition of an 'overlap' region where both scaling laws are valid. Since S_i will increase drastically for large values of y for given δ^+, and S_o will increase for small values of y, an 'overlap' region exists only if there exists a region for which both S_i and S_o remain small simultaneously. In the following paragraphs, this condition will be used in conjunction with equation (8.1) to derive the functional form of the velocity in the overlap region at finite Reynolds number.

Because of the movement of the matched layer away from the wall with increasing x, it is convenient and necessary to introduce an intermediate variable $\tilde{y}$ which can be fixed in the overlap region all the way to the limit, regardless of what is happening in physical space (see Cole & Kevorkian 1981). A definition of $\tilde{y}$ which accomplishes this is given by

$$\tilde{y} = y^+ \delta^{+-m} \tag{A 3}$$

or

$$y^+ = \tilde{y}\delta^{+m}. \tag{A 4}$$

Since $\bar{y} = y^+/\delta^+$, it follows that

$$\bar{y} = \tilde{y}\delta^{+m-1}. \tag{A 5}$$

For all values of m satisfying $0 < m < 1$, $\tilde{y}$ can remain fixed in the limit as $\delta^+ \to \infty$ while $\bar{y} \to 0$ and $y^+ \to \infty$. Substituting these into equation (8.1) yields the matching condition on the velocity as

$$f_o(\tilde{y}\delta^{+m-1}, \delta^+) = g(\delta^+) f_i(\tilde{y}\delta^{+m}, \delta^+). \tag{A 6}$$

Now equation (A 6) can be differentiated with respect to δ^+ for fixed $\tilde{y}$ to yield equations which explicitly include S_i and S_o. The result is

$$\frac{\partial f_o}{\partial \bar{y}}\bigg|_{\delta^+} \frac{\partial \bar{y}}{\partial \delta^+} + \frac{\partial f_o}{\partial \delta^+}\bigg|_{\bar{y}} = \frac{\mathrm{d}g}{\mathrm{d}\delta^+} f_i + g\left\{ \frac{\partial f_i}{\partial y^+}\bigg|_{\delta^+} \frac{\partial y^+}{\partial \delta^+} + \frac{\partial f_i}{\partial \delta^+}\bigg|_{y^+} \right\}. \tag{A 7}$$

Carrying out the indicated differentiation of y^+ and $\bar{y}$ by δ^+ (for fixed $\tilde{y}$), and

multiplying by δ^+/f_o yields (after some rearranging)

$$(m-1)\frac{\bar{y}}{f_o}\frac{\partial f_o}{\partial \bar{y}}\bigg|_{\delta^+} - m\frac{y^+}{f_i}\frac{\partial f_i}{\partial y^+}\bigg|_{\delta^+} = \frac{\delta^+}{g}\frac{\mathrm{d}g}{\mathrm{d}\delta^+} + \delta^+\left\{\frac{1}{f_i}\frac{\partial f_i}{\partial \delta^+}\bigg|_{y^+} - \frac{1}{f_o}\frac{\partial f_o}{\partial \delta^+}\bigg|_{\bar{y}}\right\}. \quad \text{(A 8)}$$

It follows immediately from equation (8.3) that

$$\frac{\bar{y}}{f_o}\frac{\partial f_o}{\partial \bar{y}}\bigg|_{\delta^+} = -\frac{\delta^+}{g}\frac{\mathrm{d}g}{\mathrm{d}\delta^+} - \delta^+\left\{\frac{1}{f_i}\frac{\partial f_i}{\partial \delta^+}\bigg|_{y^+} - \frac{1}{f_o}\frac{\partial f_o}{\partial \delta^+}\bigg|_{\bar{y}}\right\}. \quad \text{(A 9)}$$

Equation (A 9) can be rewritten as

$$\frac{\bar{y}}{f_o}\frac{\partial f_o}{\partial \bar{y}}\bigg|_{\delta^+} = \gamma(\delta^+) - \delta^+(S_i - S_o) \quad \text{(A 10)}$$

where $\gamma = \gamma(\delta^+)$ is defined by

$$\gamma(\delta^+) \equiv -\frac{\delta^+}{g}\frac{\mathrm{d}g}{\mathrm{d}\delta^+} = -\frac{\mathrm{d}\ln g}{\mathrm{d}\ln \delta^+}. \quad \text{(A 11)}$$

Note that the first term on the right-hand side of (A 10) is at most a function of δ^+ alone, while the second term contains all of the residual y-dependence.

Now it is clear that if both

$$|S_o| \ll \left|\frac{1}{\delta^+}\frac{\mathrm{d}\ln g}{\mathrm{d}\ln \delta^+}\right| = \left|\frac{\gamma}{\delta^+}\right| \quad \text{(A 12)}$$

and

$$|S_i| \ll \left|\frac{1}{\delta^+}\frac{\mathrm{d}\ln g}{\mathrm{d}\ln \delta^+}\right| = \left|\frac{\gamma}{\delta^+}\right| \quad \text{(A 13)}$$

then the first term on the right-hand side of equation (A 9) dominates. If $\gamma \to$ constant as $\delta^+ \to \infty$, the inequalities are satisfied. Note that a much weaker condition can be applied which yields the same result, namely that both inner and outer scaled profiles have the same dependence on δ^+, i.e. $S_i = S_o$ in the overlap range.

Since these inequalities are satisfied over some range in y, then to leading order, equation (A 9) can be written as

$$\frac{\bar{y}}{f_o^{(1)}}\frac{\partial f_o^{(1)}}{\partial \bar{y}}\bigg|_{\delta^+} = \gamma(\delta^+). \quad \text{(A 14)}$$

The solution to equation (A 14) can be denoted as $f_o^{(1)}$ since it represents a first-order approximations to f_o. It is not, however, simply the same as $f_{o\infty}$ because of the δ^+ dependence of γ, but reduces to it in the limit. Thus, by regrouping into the leading term all of the y-independent contributions, the method applied here has yielded a more general result than the customary expansion about infinite Reynolds number. It is also easy to see why the usual matching of infinite Reynolds number inner and outer solutions will not work if the limiting value of γ is zero.

From equation (8.3), it also follows that

$$\frac{y^+}{f_i^{(1)}}\frac{\partial f_i^{(1)}}{\partial y^+}\bigg|_{\delta^+} = \gamma(\delta^+). \quad \text{(A 15)}$$

An interesting feature of these first-order solutions is that the inequalities given by equations (A 12) and (A 13) determine the limits of validity of both equations (A 14)

and (A 15) since either S_o or S_i will be large outside the overlap region. Clearly the extent of this region will increase as the Reynolds number (or δ^+) increases.

Both equations (A 14) and (A 15) must be independent of the origin for y, i.e. invariant to transformations of the form $y \to y + a$. Therefore, the most general solutions are of the form

$$f_o^{(1)}(\bar{y}, \delta^+) = C_o(\bar{y} + \bar{a})^\gamma, \tag{A 16}$$

$$f_i^{(1)}(y^+, \delta^+) = C_i(y^+ + a^+)^\gamma, \tag{A 17}$$

where the parameters C_o, C_i and γ are functions of δ^+ and must be determined along with the constant a. In the remainder of this paper, the superscript (1) will be dropped; however it is these first-order solutions that are being referred to unless otherwise stated.

The relation between u_* and U_m follows immediately from equation (8.1), i.e.

$$g(\delta^+) = \frac{C_o(\delta^+)}{C_i(\delta^+)} \delta^{+-\gamma(\delta^+)}. \tag{A 18}$$

However, equation (A 11) must also be satisfied. Substituting equation (A 18) into (A 11) implies that γ, C_o, and C_i are constrained by

$$\ln \delta^+ \frac{\mathrm{d}\gamma}{\mathrm{d}\delta^+} = \frac{\mathrm{d}}{\mathrm{d}\delta^+} \ln \left[\frac{C_o}{C_i} \right] \tag{A 19}$$

or equivalently,

$$\ln \delta^+ \frac{\mathrm{d}\gamma}{\mathrm{d} \ln \delta^+} = \frac{\mathrm{d}}{\mathrm{d} \ln \delta^+} \ln \left[\frac{C_o}{C_i} \right]. \tag{A 20}$$

Equation (A 19) is exactly the criterion for the neglected terms in (A 9) to vanish identically (i.e. $S_i - S_o \equiv 0$). Therefore the solution represented by equations (A 16)–(A 19) is, indeed, the first-order solution for the velocity profile in the overlap layer at finite, but large, Reynolds number. Clearly when y^+ is too big or $\bar{y}$ is too small for a given value of δ^+, the inequalities of equations (A 12) and (A 13) cannot be satisfied. Since all the derivatives with respect to δ^+ must vanish as $\delta^+ \to \infty$ (the AIP), the inner range of the outer overlap solution is unbounded in the limit, as is the outer range of the inner.

Since equation (A 20) must be satisfied regardless of the precise choice of δ^+, solutions to it must be invariant to transformations of the type $\delta^+ \to D\delta^+$ where D is a scale factor. Also, equations (A 16) and (A 17) must be asymptotically independent of Reynolds number, since f_i and f_o are. Therefore the coefficients and exponent must be asymptotically constant, i.e.

$$\gamma(\delta^+) \to \gamma_\infty,$$

$$C_o(\delta^+) \to C_{o\infty},$$

$$C_i(\delta^+) \to C_{i\infty},$$

as $\delta^+ \to \infty$. Also, as noted in § 8, γ_∞, $C_{o\infty}$ and $C_{o\infty}$ cannot be zero. These conditions are powerful constraints; and together with equation (A 19) rule out some functional forms for γ (like that suggested by Barenblatt (1993), for example). Therefore it is important to note that they are a direct consequence of the AIP and the assumption that scaling laws should correspond to similarity solutions of the equations of motion.

Appendix B. The Reynolds stress in the overlap layer

By following the same procedure as for the velocity (see Appendix A), the outer and inner Reynolds stress profile functions for the overlap region can be obtained (just as for the boundary layer by GC). Here, the Reynolds shear stress is given by

$$r_o(\bar{y};\delta^+) = D_o(\delta^+)\bar{y}^{\beta(\delta^+)}, \tag{B 1}$$

$$r_i(y^+;\delta^+) = D_i(\delta^+)y^{+\beta(\delta^+)}, \tag{B 2}$$

where a solution is possible only if

$$\frac{R_{so}}{R_{si}} = \frac{D_i}{D_o}\delta^{+\beta} \tag{B 3}$$

and

$$\ln\delta^+\frac{\mathrm{d}\beta}{\mathrm{d}\delta^+} = \frac{\mathrm{d}}{\mathrm{d}\delta^+}\ln\left[\frac{D_o}{D_i}\right]. \tag{B 4}$$

Unlike the velocity, however, more information about the Reynolds stress is available from the averaged momentum equation for the overlap layer since both equations (2.4) and (2.5) reduce to

$$\frac{\partial}{\partial y}\langle -uv\rangle = 0 \tag{B 5}$$

in the limit of infinite Reynolds number. Thus,

$$\beta R_{so}D_o\bar{y}^{\beta-1} \to 0 \tag{B 6}$$

and

$$\beta R_{si}D_i y^{+\beta-1} \to 0. \tag{B 7}$$

Since both D_o and D_i must remain finite and be asymptotically constant (if the Reynolds stress itself is non-zero), these conditions can be met only if

$$\beta \to 0. \tag{B 8}$$

From equation (B 5) for large values of y^+, the Reynolds stress in inner variables in the matched layer is given to first order (exact in the limit) by

$$r_i \to 1. \tag{B 9}$$

Since $R_{si} = u_*^2$, this can be consistent with equation (B 2) only if $D_i \to 1$ as $\delta^+ \to \infty$. It follows immediately that

$$R_{so} \to \frac{D_i}{D_o}u_*^2 \tag{B 10}$$

in the infinite Reynolds number limit, just as suggested in § 5.

Appendix C. The effect of Reynolds number on the overlap range

This Appendix also parallels very closely GC, but is included here since it is also important to understanding the wall jet. The overlap layer can be related directly to the averaged equations for the mean flow and the Reynolds stresses. The latter will be seen to be of particular interest since it is through them that the local Reynolds number influences the approach to the asymptotic state. Of particular interest is the question of how large the Reynolds number must be before the wall jet begins to show the characteristics of the asymptotic state.

The averaged momentum equation from about $y^+ > 30$ out to $\bar{y} < 0.1$ is given approximately by

$$0 = \frac{\partial}{\partial y}\langle -uv \rangle. \tag{C 1}$$

It has no obvious Reynolds number dependence; and the stress is effectively constant throughout this region. This is, however, not the entire story because of the Reynolds transport equations. For this 'constant shear stress region' the viscous diffusion and mean convection terms are negligible (as in the mean momentum equation), so the equations reduce approximately to (Tennekes & Lumley 1972)

$$0 = -\left(\left\langle p\frac{\partial u_i}{\partial x_k}\right\rangle + \left\langle p\frac{\partial u_k}{\partial x_i}\right\rangle\right) - \left[\langle u_i u_2\rangle\frac{\partial U_k}{\partial x_2} + \langle u_k u_2\rangle\frac{\partial U_i}{\partial x_2}\right] - \frac{\partial\langle u_i u_k u_2\rangle}{\partial x_2} - 2\epsilon_{ik}, \tag{C 2}$$

where $U_i = U\delta_{i1}$. Thus the viscosity does not appear directly in any of the single-point equations governing this region, nor does it appear in those governing the outer boundary layer.

In spite of the above, viscosity continues to play a crucial role in at least a portion of the constant stress layer, even at infinite Reynolds number. The reason for this is that the scales at which the dissipation, ϵ_{ik}, takes place depend on the local turbulence Reynolds number, $R_t = u'L/\nu$. For $R_t > 10^4$ approximately, the energy dissipation is completely controlled by the large energetic scales of motion. These are effectively inviscid, but transfer energy through nonlinear interactions (the energy cascade) to the much smaller viscous scales where the actual dissipation occurs (see Tennekes & Lumley 1972). When this is the case, the dissipation is nearly isotropic so $\epsilon_{ik} \approx \epsilon\delta_{ik}$. Moreover, ϵ can be approximated by the infinite Reynolds number relation: $\epsilon \sim q^3/L$, where L is a scale characteristic of the energy-containing eddies. Thus the entire Reynolds stress equations are effectively inviscid. Note that in this limit the Reynolds shear stress has no dissipation at all, i.e. $\epsilon_{12} = 0$.

At very low turbulence Reynolds number, however, the dissipative and energy-containing scales nearly overlap, and so the latter (which also produce the Reynolds shear stress) feel directly the influence of viscosity. In this limit, the energy and dissipative ranges nearly overlap, and the dissipation is more reasonably estimated by $\epsilon \sim \nu q^2/L^2$, where the constant of proportionality is of order 10. The dissipation tensor, ϵ_{ik}, is anisotropic and ϵ_{12}, in particular, is non-zero (Hanjalic & Launder 1974).

For turbulence Reynolds numbers between these two limits, the dissipation will show characteristics of both limits, gradually making a transition from $\epsilon \sim \nu q^2/L^2$ to $\epsilon \sim q^3/L$ as R_t increases. Thus the Reynolds stresses themselves will feel this directly, and will show a strong Reynolds number dependence. Obviously, in order to establish when (if at all) parts of the flow become Reynolds number independent, it is necessary to determine how the local turbulence Reynolds number varies downstream and across the flow.

Over the outer boundary layer (which is most of it) and excluding the overlap region, $L \approx 0.65y_{1/2}$ and $u' \approx 0.2U_m$. So when $U_m y_{1/2}/\nu > 7000$, the dissipation in the outer flow is effectively inviscid. The data of KEP vary from 14×10^3 at $x/b = 20$ to 31×10^3 at $x/b = 150$. Hence the mean and turbulence quantities in the outer flow should show little Reynolds number dependence, and this is indeed the case – when they are scaled properly! They can, of course, not be entirely Reynolds number independent because of the boundary conditions imposed by the inner flow on the outer. This residual dependence manifests itself in the overlap layer in the slow variations of C_i and γ, for example.

The near-wall region is considerably more interesting, however, since in it the scales governing the energy-containing eddies are constrained by the proximity of the wall. Hence, the turbulence Reynolds number, R_t, depends on the distance from the wall, y. In fact, $R_t \sim y^+$ with a coefficient of about 18, so in effect y^+ is the turbulence Reynolds number. Because of this, two things are immediately obvious.

First, since the physical distance from the wall for a fixed value of y^+ does not increase with downstream distance as rapidly as the jet spreads, then more and more of the wall jet will become effectively inviscid and will be governed by the inviscid dissipation relation. And correspondingly, the mean and turbulence quantities in the overlap layer will become Reynolds number independent, albeit very slowly. This is exactly the physical reason why C_o, C_i, and γ become asymptotically constant as described above. And clearly these limiting values cannot be reached until the entire 'inertial' layer is governed by the infinite Reynolds number dissipation relation. Obviously this can happen only when there is a substantial range satisfying $y^+ > 300$ and for which the mean convection terms are negligible. Thus the asymptotic limits are realized only when $300\nu/u_* \ll 0.1y_{1/2}$ or $u_* y_{1/2}/\nu \gg 3000$, which corresponds approximately to $U_m y_{1/2}/\nu \gg 50\,000$. This is well above the range of the data considered here, or available elsewhere. Therefore the overlap layer, to the extent that it is identifiable at all, should (and does) display a Reynolds number dependence, not only in C_o, C_i, and γ, but correspondingly in the behaviour of $\langle u^2 \rangle$, $\langle uv \rangle$, etc. This is directly analogous to the observations in the zero-pressure-gradient boundary layer (cf. Gad-el-Hak & Bandyopadhyay 1994; GC).

Second, there will always be a mesolayer (a term appropriated from Long & Chen (1981) who argued for its existence, but from entirely different physical and scaling arguments which we find untenable) a region below about $y^+ \approx 300$ in which the dissipation can never assume the character of a high Reynolds number flow. Hence, the dissipation can never become independent of viscosity, no matter how high the Reynolds number becomes – and even though the mean momentum equation itself is inviscid above $y^+ \approx 30$! This is well-known to turbulence modellers, but the consequences for similarity theory and asymptotic analyses do not seem to have been noticed previously. It is particularly important for experimentalists who have routinely (and wrongly) tried to apply asymptotic formulas to data from to this region.

Thus the constant stress layer is really four separate regions, each having its own unique character: the 'inertial' layer ($y^+ > 300, \bar{y} < 0.1$) obtained in the preceding section which can ultimately become inviscid; an 'in-between layer' ($30 < y^+ < 300$), in which the viscous stresses are negligible, but in which viscosity acts directly on the turbulence scales producing the Reynolds stresses; a buffer layer ($3 < y^+ < 30$ approximately) where the Reynolds stress and viscous stress both control the mean flow; and the linear sublayer near the wall ($y^+ < 3$ approximately) where the viscous stresses dominate. It seems appropriate to call this 'in-between layer' the mesolayer since it is clearly not the buffer layer, nor is it the overlap region. And unlike the 'mesolayer' proposed by Long & Chen (1981), it needs no new length scale to describe it since its characteristics and extent are measured entirely by y^+. Interestingly, the application of near-asymptotics to the overlap region appears to capture the functional dependence of both the inertial and mesolayer regions with the offset parameter a as noted in § 11.

REFERENCES

Abrahamsson, H., Johansson, B. & Löfdahl, L. 1994 A turbulent plane two-dimensional wall-jet in a quiescent surrounding. *Eur. J. Mech.* B/*Fluids* **13**, 533–556 (referred to herein as AJL).

Barenblatt, G. I. 1993 Scaling laws for fully developed shear flow. Part 1. Basic hypotheses and analysis. *J. Fluid Mech.* **248**, 513–520.

Bradshaw, P. & Gee, M. 1960 Turbulent wall jets with and without an external stream. *Aero. Res. Council R & M*.

Castillo, L. 1997 Similarity analysis of turbulent boundary layers. PhD thesis, University at Buffalo.

Cole, J. D. & Kevorkian, J. 1981 *Perturbation Methods in Applied Mathematics*. Springer.

Eriksson, J., Karlsson, R. & Persson, J. 1998 An experimental study of a two-dimensional plane turbulent wall jet. *Expts. Fluids* **25**, 50–60 (referred to herein as EKP).

Gad-el-Hak, M. & Bandyopadhyay, P. R. 1994 Reynolds number effects in wall-bounded flows. *Appl. Mech. Rev.* **47**, 307–365.

George, W. K. 1989 The self-preservation of turbulent flows and its relation to initial conditions and coherent structures. In *Advances in Turbulence* (ed. W. George & R. Arndt), pp. 39–73. Hemisphere.

George, W. K. 1992 The decay of homogeneous isotropic turbulence. *Phys. Fluids* A **4**, 1492–1509.

George, W. K. 1995 Some new ideas for similarity of turbulent shear flows. In *Proc. ICHMT Symposium on Turbulence, Heat and Mass Transfer, Lisbon, Portugal (1994)* (ed. K. Hanjalic & J. Pereira). Begell House.

George, W. K. & Castillo, L. 1997 Zero-pressure-gradient turbulent boundary layer. *Appl. Mech. Rev.* **50**, 689–729 (referred to herein as GC).

George, W. K. & Gibson, M. M. 1992 The self-preservation of homogeneous shear flow turbulence. *Expts. Fluids* **13**, 229–238.

Hanjalic, K. & Launder, B. E. 1974 Contribution towards a Reynolds stress closure for low-Reynolds number turbulence. *Rep.* HTS/74/24. Imperial College.

Irwin, H. 1973 Measurements in a self-preserving plane wall jet in a positive pressure gradient. *J. Fluid Mech.* **61**, 33–63.

Johansson, T. & Karlsson, R. 1989 Energy budget in the near-wall region of a turbulent boundary layer. In *Applications of Laser Anemometry to Fluid Mechanics* (ed. R. Adrian, T. Asanuma, D. Durão, F. Durst & J. Whitelaw), pp. 3–22. Springer.

Karlsson, R., Eriksson, J. & Persson, J. 1993*a* An experimental study of a two-dimensional plane turbulent wall jet. *Tech. Rep.* VU-S93-B36. Vattenfall Utveckling AB, Älvkarleby Laboratory, Sweden (referred to herein as KEP).

Karlsson, R., Eriksson, J. & Persson, J. 1993*b* LDV measurements in a plane wall jet in a large enclosure. In *Laser Techniques and Application in Fluid Mechanics* (ed. R. Adrian, D. Durão, F. Durst, M. Heitor, M. Maeda & J. Whitelaw), pp. 311–332. Springer.

Kobayashi, R. & Fujisawa, N. 1982 Turbulence characteristics of plane wall jets. *Rep. Inst. High Speed Mech., Tohoku University*, vol. 45, pp. 95–114.

Launder, B. E. & Rodi, W. 1981 The turbulent wall jet. *Prog. Aerospace Sci.* **19**, 81–128.

Launder, B. E. & Rodi, W. 1983 The turbulent wall jet – measurements and modelling. In *Ann. Rev. Fluid Mech.* **15**, 429–459.

Long, R. R. & Chen, T.-C. 1981 Experimental evidence for the existence of the 'mesolayer' in turbulent systems. *J. Fluid Mech.* **105**, 19–59.

Moser, R., Rogers, M. & Ewing, D. 1998 Self-similarity of time-evolving plane wakes. *J. Fluid Mech.* **367**, 255–289.

Narasimha, R., Yegna Narayan, K. & Parthasarathy, S. 1973 Parametric analysis of turbulent wall jets in still air. *Aero. J.* pp. 355–359.

Oberlack, M. 1997 Unified theory for symmetries in plane parallel turbulent shear flows. Manuscript 163. Center for Turbulence Research, NASA Ames/Stanford University (also submitted to *J. Fluid Mech.*).

Tennekes, H. & Lumley, J. L. 1972 *A First Course in Turbulence*. MIT Press.

Townsend, A. A. 1976 *The Structure of Turbulent Shear Flow*, 2nd edn. Cambridge University Press.

Wygnanski, I., Champagne, F. & Marasli, B. 1986 On the large-scale structures in two-dimensional, small-deficit, turbulent wakes. *J. Fluid Mech.* **168**, 31–71.

Wygnanski, I., Katz, Y. & Horev, E. 1992 On the applicability of various scaling laws to the turbulent wall jet. *J. Fluid Mech.* **234**, 669–690 (referred to herein as WKH).